Beam Heating of the Neutralizer Gas of Neutral Beam Injectors

W. Ott

IPP 4/237 February 1989

Max-Planck-Institut für Plasmaphysik
Euratom Association, D-8046 Garching bei München

MAX-PLANCK-INSTITUT FÜR PLASMAPHYSIK

8046 GARCHING BEI MÜNCHEN

Beam Heating of the Neutralizer Gas of Neutral Beam Injectors

W. Ott

IPP 4/237 February 1989

Max-Planck-Institut für Plasmaphysik
Euratom Association, D-8046 Garching bei München

Abstract

It was shown by Paméla /1-2/ that the target thickness of the neutralizer gas in neutral beam injectors is smaller than to be expected from gas flow calculations. He explained his findings by direct and indirect beam heating of the gas and a consequent flow acceleration. The role of the neutralizer plasma electrons in the gas heating scenario is reconsidered here. To this end the particle and energy balances of the electrons are solved with allowance for ionization and dissociation of the gas by the electrons. It is shown that the direct contribution of the electrons to heating is not dominant. Their indirect contribution via ion acceleration in the space charge sheath in front of the walls is usually stronger. Methods to increase the neutralizer target thickness are investigated. They are essentially (1) structuring the neutralizer surface in order to reduce the reflection of medium energy particles and to increase the gas accommodation, (2) cooling down the neutralizer to LN_2-temperature. The scaling of the target thickness with various parameters is investigated and compared with "cold" flow.

Initially it was assumed that the neutralizer plasma electrons are hot and able to excite Balmer alpha radiation in collisions with H_2 molecules. The investigation shows that the electrons must be cold instead ($T_e < 5\,\mathrm{eV}$). An enhanced emission of the unshifted Balmer alpha line as measured on the IPP test bed is probably caused by dissociative recombination of H_2^+ and H_3^+ ions leading to excited hydrogen atoms.

Die nachstehende Arbeit wurde im Rahmen des Vertrages zwischen dem Max-Planck-Institut für Plasmaphysik und der Europäischen Atomgemeinschaft über die Zusammenarbeit auf dem Gebiet der Plasmaphysik durchgeführt

Contents

1. Introduction 1
2. Model of the neutralizer plasma 1
3. Gas heating model 5
4. Gas flow and target thickness 6
5. How to keep the neutralizer gas cooler? 10
6. Scaling considerations 11
7. What is the cause for the enhanced emission of unshifted H_α radiation? 12

Appendix I: Coulomb heating of the neutralizer plasma by the beam ... 13

Appendix II: Cross section σ_{ib} 14

Appendix III: ASDEX UPGRADE neutralizers 15

References 16

List of symbols 17

Figure captions 19

Figures 1 ... 18

1. Introduction

Spectroscopic measurements were made on the test bed for the IPP hydrogen neutral beam injectors in the spectral range around the Balmer-alpha line. The aim was to determine the species ratio of full, half and third-energy particles in the beam which are the breakup products of H^+, H_2^+ and H_3^+. The Doppler-shifted spectra can be evaluated using the cross-sections for Balmer-alpha emission of beam and target particles reported by Williams et al. /3/. The optical species measurements are dealt with elsewhere. This paper starts from the observation that in spectra taken from the neutralizer light the unshifted line is about five times stronger than the sum of the shifted lines. The Williams cross-sections suggest a ratio unshifted : shifted of about 1 : 2. Measurements in the target tank on the other hand showed an unshifted line intensity in accordance with /3/. The different spectra are shown in **Figure 1.**

It may be assumed that the difference is caused by the electrons of the neutralizer plasma. Now, if these electrons excite an energy level 12.1 eV above the ground state, the question arises what effect they have on ionization, dissociation and heating of the neutralizer gas. In plasma physics, H_α emission is usually taken as an indicator of hydrogen ionization (see e.g. /4/). The present report shows that the opposite may be true.

In this paper first the neutralizer plasma is dealt with in order to calculate the electron density and temperature. These are used to calculate the gas temperature which enters into the gas flow calculations. Two integrations give the gas density as a function of the position within the neutralizer and the gas target thickness. A parameter study shows the relative importance of the different heating mechanisms. Several methods to increase the gas target thickness for a given gas flow are proposed. A final section deals with possible reactions leading to unshifted Balmer-alpha emission.

2. Model of the neutralizer plasma

The neutralizer plasma is mainly described by the density and temperature of the electrons and by the kind of ions being present. This plasma is similar to the positive column of a low-pressure discharge: The electrons have a much higher temperature than the ions. The fastest electrons leave the plasma quickly and create a positive plasma potential which confines the rest of the electrons. The ions are confined "inertially" and accelerated to the walls by this positive plasma potential. A small potential drop occurs within the plasma, the main drop, however,within a thin sheath in front of the boundary walls whose thickness is several times the Debye length.

To obtain the energy balance of the neutralizer electrons, we must know the average energy with which they are created. A single value is known to the author: Gibson /5/ made extensive measurements of the energy distribution of electrons created in collisions of 50 keV protons with hydrogen gas. So we limit ourselves to a single-species H^+/H^0 beam of this energy and take Gibson's value $E_s = 22.4\,\mathrm{eV}$ /6/ as the initial energy of the electrons. In the W7AS and ASDEX injectors we have comparable design energies (45 and 55 keV, respectively), although only about 50% atomic species.

Further simplifications of this treatment are

- the only plasma ions included are H_2^+ ions; all reactions leading to H^+ and H_3^+ are neglected,
- the beam space charge is neglected,
- the charge deposition of the beam into the neutralizer is neglected,
- the neutralizer wall is at floating potential,
- the self-interaction of the electrons creates a Maxwellian energy distribution with a temperature T_e,
- the neutralizer is a circular cylinder of diameter d and length l.

We may then use the Bohm criterion /7/, which is consistent with much more refined calculations (Scheuer and Emmert /8/), and calculate the ion current density to the wall

$$
\begin{aligned}
j_i &= \exp(-\frac{1}{2})\, e\, n_e \sqrt{\frac{kT_e}{m_i}} \\
&= 0.95 \times 10^{-13}\, n_e \sqrt{\frac{T_e}{M_i}}, \qquad \left[\frac{\mathrm{A}}{\mathrm{cm}^2}, \mathrm{cm}^{-3}, \mathrm{eV}\right]
\end{aligned} \tag{1}
$$

(Ott /9/). This gives a floating potential of

$$
\begin{aligned}
U_f &= -\frac{kT_e}{2e}(1 + \ln \frac{m_i}{2\pi m_e}) \\
&= -\,T_e\,(3.34 + 0.5 \ln M_i), \qquad [\mathrm{V}, \mathrm{eV}] \\
&= -\,3.69\,T_e \qquad \text{for} \quad M_i = 2
\end{aligned} \tag{2}
$$

and a confinement time for ions and electrons

$$
\begin{aligned}
\tau &= \frac{\exp \frac{1}{2}}{4}\, d \sqrt{\frac{m_i}{kT_e}} \\
&= 4.2 \times 10^{-7}\, d \sqrt{\frac{M_i}{T_e}}, \qquad [\mathrm{s}, \mathrm{cm}, \mathrm{eV}].
\end{aligned} \tag{3}
$$

We balance the charged particle density between ionization due to the beam and electrons and losses due to the wall current:

$$
\sigma_{ib} n I_b + e n_e n \langle \sigma_i v_e \rangle \frac{\pi}{4} d^2 = \pi d\, j_i
$$

with

σ_{ib} cross-section for H_2^+ formation in *proton* collisions with H_2 molecules,

σ_i cross-section for H_2^+ formation in *electron* collisions with H_2 molecules,

n gas density,

I_b beam current.

This gives the electron density

$$n_e = \frac{\sigma_{ib} n I_b}{\pi d e \left[\exp(-\frac{1}{2})\sqrt{\frac{kT_e}{m_i}} - \frac{1}{4} n d \langle \sigma_i v_e \rangle\right]}$$

$$= \frac{7.96 \times 10^{18} \frac{\sigma_{ib} I_b}{d^2} n}{\frac{2.38 \times 10^6}{d}\sqrt{\frac{T_e}{M_i}} - \langle \sigma_i v_e \rangle \, n}, \quad \left[\mathrm{cm}^{-3}, \mathrm{cm}^2, \mathrm{A}, \mathrm{cm}, \mathrm{eV}, \frac{\mathrm{cm}^3}{\mathrm{s}}\right]. \tag{4}$$

In this equation, resulting from the particle balance, n_e and T_e are still interlinked. A second relation has to be derived from the *energy* balance.

Sources of electron energy included are the birth energy of $E_s = 22.4\,\mathrm{eV}$ and Coulomb heating by the beam. Coulomb heating is treated in Appendix I and is included in the balance equation although only an energy of $\approx 0.5\,\mathrm{eV}$ is gained by the electrons during an average lifetime τ. The main energy *loss* of the electrons is due to wall collisions. The space charge sheath in front of the wall repels the electrons. Their density decreases steadily with the potential and at the wall has fallen by the Boltzmann factor $\exp(eU_f/kT_e)$. The average kinetic energy of the electrons is independent of the potential (in first approximation because backstreaming electrons are missing). The total energy loss for the electron gas by one electron hitting the wall is this average kinetic energy $\frac{3}{2}kT_e$ plus the potential eU_f it has gained in the sheath. This potential energy is transferred to the ions, which transport it also to the wall.

Additional electron energy losses included in the balance are dissociative ($E_d \approx -10\,\mathrm{eV}$, Janev /10/) and ionizing ($E_i = -15.4\,\mathrm{eV}$) collisions with H_2 molecules.

The electron energy balance (divided by n_e) may thus be written as

$$\frac{\sigma_{ib} n I_b E_s}{e n_e} + \frac{2\pi e^3}{(4\pi\epsilon_0)^2}\frac{\mathrm{M}(x_\beta)\lambda_{ie} m_i \xi I_b}{m_e E_b}$$

$$= \frac{\pi}{2\exp\frac{1}{2}} \frac{(4 + \ln\frac{m_i}{2\pi m_e})\, d\,(kT_e)^{\frac{3}{2}}}{\sqrt{m_i}} + \frac{\pi}{4} d^2 n (E_i \langle \sigma_i v_e \rangle + E_d \langle \sigma_d v_e \rangle). \tag{5}$$

($\mathrm{M}(x_\beta)$, λ_{ie} see Appendix I, ξ = average charge fraction of the beam)

Like equation (4) also equation (5) combines n_e and T_e. From both equations n_e may be eliminated, yielding a unique function $T_e = T_e(n)$ in implicit form:

$$n = \frac{\exp(-\frac{1}{2})\, d \sqrt{\frac{kT_e}{m_i}}\left[E_s - (2 + 0.5\ln\frac{m_i}{2\pi m_e})kT_e\right] + \frac{2e^3}{(4\pi\epsilon_0)^2}\frac{\mathrm{M}(x_\beta)\lambda_{ie} I_b}{E_b}\frac{m_i}{m_e}}{\frac{d^2}{4}\left[(E_s + E_i)\langle \sigma_i v_e \rangle + E_d \langle \sigma_d v_e \rangle\right]}$$

$$= \frac{2.38 \times 10^6 d \sqrt{\frac{T_e}{M_i}}\left[(E_s - (4.84 + 0.5\ln Mi)T_e\right] + 1.91 \times 10^9 \frac{\mathrm{M}(x_\beta)\lambda_{ie} I_b M_i}{E_b}}{d^2\left[(E_s + E_i)\langle \sigma_i v_e \rangle + E_d \langle \sigma_d v_e \rangle\right]}, \tag{6}$$

$$\left[\mathrm{cm}^{-3}, \mathrm{cm}, \mathrm{eV}, \mathrm{A}, \frac{\mathrm{cm}^3}{\mathrm{s}}\right].$$

If T_e were determined by the initial energy of the electrons and the wall losses only (no Coulomb heating, no ionization and dissociation by the secondary electrons), we would obtain

$$T_{es} = \frac{2E_s}{4 + \ln \frac{m_i}{2\pi m_e}}$$

$$= \frac{2E_s}{9.68 + \ln M_i} \tag{7a}$$

$$= 4.3\text{eV} \quad \text{for } M_i = 2 \text{ and } E_s = 22.4\text{eV}$$

independently of the gas density, and

$$n_{es} = \frac{\exp(\frac{1}{2})\sigma_{ib} I_b n}{\pi e d} \sqrt{\frac{m_i}{kT_e}}$$

$$= 3.345 \times 10^{12} \frac{\sigma_{ib} I_b n}{d} \sqrt{\frac{M_i}{T_e}}, \qquad [\text{cm}^{-3}, \text{cm}^2, \text{A}, \text{cm}, \text{eV}] \tag{7b}$$

$$= 2.28 \times 10^{12} \frac{\sigma_{ib} I_b n}{d} \quad \text{for} \quad M_i = 2.$$

A computer program was written solving equation (6) $n = n(T_e)$ and subsequently equation (4) $n_e = n_e(T_e)$. The reaction rate coefficients for electron ionization and dissociation are taken from the recent collection of Janev et al. /10/. The value for the cross section σ_{ib} to be taken is dealt with in Appendix II. The results of the computations are displayed in graphical form: **Figures 2** and **3** show $n_e = n_e(n)$ for the geometries and the beam current typical of the existing injectors for ASDEX/W7AS and the injector designed for ASDEX UPGRADE[1]. The beam density n_b is also drawn. Our treatment is invalid in the low $10^{12}\,\text{cm}^{-3}$ range of n because n_e must be higher than n_b. The dashed curve shows the electron density according to equation (7b). The figures show that the main effects determining the electron density are direct beam ionization and the losses to the wall. Dissociation and ionization by the beam electrons give minor corrections only. Finally, Paméla's electron density (equation B13 of the appendix of /1/) is also shown. These values are obviously a factor of 2 to 5 too high.

The electron temperature T_e is shown in **Figure 4** as a function of the neutral gas density n together with the value of T_{es} according to equation (7a). T_e is higher than T_{es} for very low values of n. Here we see the small effect of Coulomb heating. For higher values of n cooling by inelastic collisions becomes more and more effective.

[1]The neutralizers of the ASDEX/W7AS injectors are in fact circular cylinders as assumed here. The neutralizer of the ASDEX UPGRADE injector has a very complicated shape. How the shape is translated into a circular cylinder is shown in Appendix III.

3. Gas heating model

Paméla /1, 2/ has shown that direct collisional energy transfer from beam ions or secondary electrons to the gas is small and that gas heating via heavy particles in the 1 eV energy range, on the other hand, is very effective. A collision cross section of $\sigma_{tr}^0 = 5 \times 10^{-16}\text{cm}^2$ for H^0 or H_2^0 and of $\sigma_{tr}^+ = 1 \times 10^{-15}\text{cm}^2$ for H^+ and the factors

$$f_{tr}^0 = 1 - \exp(-\sigma_{tr}^0 nd)$$
$$f_{tr}^+ = 1 - \exp(-\sigma_{tr}^+ nd)$$

are taken for the efficiency of the energy transfer from these particles to the gas. Three processes have been proposed by Paméla:

1. The H_2 gas molecules may be dissociated by the beam protons. The different collision processes treated by Paméla may be summarized by

$$\underline{H^+}(50\,\text{keV}) + H_2 \rightarrow \begin{cases} H^+;\ \sigma_{H^+} = 4.3 \times 10^{-17}\text{cm}^2;\ \langle E_{H^+,b}\rangle = 7.8\,\text{eV} \\ H^0;\ \sigma_{H^0} = 1.4 \times 10^{-16}\text{cm}^2;\ \langle E_{H^0,b}\rangle = 2.4\,\text{eV}. \end{cases}$$

This gives a power per unit length of the neutralizer transferred to the gas

$$\begin{aligned} p_b &= \frac{\xi I_b n}{e}(\sigma_{H^+}\langle E_{H^+,b}\rangle f_{tr}^+ + \sigma_{H^0}\langle E_{H^0,b}\rangle f_{tr}^0) \\ &= \xi I_b n(\sigma_{H^+}\langle E_{H^+,b}\rangle f_{tr}^+ + \sigma_{H^0}\langle E_{H^0,b}\rangle f_{tr}^0), \qquad \left[\frac{\text{W}}{\text{cm}}, \text{A}, \text{cm}^{-3}, \text{cm}^2, \text{eV}\right]. \end{aligned} \tag{8}$$

2. Dissociation of H_2 molecules by the secondary electrons. The rate coefficient used here is taken from Janev /10/ and also the average energy $\langle E_{H^0,e}\rangle = 2.5\,\text{eV}$ of the resulting atoms. The power per unit length is

$$\begin{aligned} p_e &= \frac{\pi}{4} d^2\, 2 n_e n \langle \sigma_d v_e\rangle \langle E_{H^0,e}\rangle f_{tr}^0 \\ &= 2.51 \times 10^{-19} d^2 n_e n \langle \sigma_d v_e\rangle \langle E_{H^0,e}\rangle f_{tr}^0, \qquad \left[\frac{\text{W}}{\text{cm}}, \text{cm}, \text{cm}^{-3}, \frac{\text{cm}^3}{\text{s}}, \text{eV}\right]. \end{aligned} \tag{9}$$

Heating connected with ionization by electrons is neglected because the corresponding rate coefficient is so small.

3. Wall reflection of ions. Ions accelerated in the boundary sheath and neutralized at the surface are reflected with a certain probability. The ion energy is determined by the floating potential U_f. Paméla's value of $r_w = 0.3$ is taken as the energy reflection probability for usual wall conditions. A value up to $r_w = 0.6$ would, however, seem reasonable as well (Eckstein /11/). The power per unit length (using equations (1) and (2)) is

$$\begin{aligned} p_w &= \pi\, d\, j_i\, |U_f|\, r_w\, f_{tr}^0 \\ &= 1.49 \times 10^{-13}\, r_w\, d\, n_e \frac{6.68 + \ln M_i}{\sqrt{M_i}} T_e^{\frac{3}{2}} f_{tr}^0, \qquad \left[\frac{\text{W}}{\text{cm}}, \text{cm}, \text{cm}^{-3}, \text{eV}\right]. \end{aligned} \tag{10}$$

With the gas temperature T, the wall temperature T_0, the accomodation factor α and the specific heat ratio γ and $\gamma - 1 = 0.4$, the power loss of the gas to the wall becomes

$$
\begin{aligned}
p_l &= \pi d \frac{n\bar{v}}{4} \frac{1}{\gamma - 1} \alpha k (T - T_0) \\
&= \frac{d\, n\, \alpha}{\gamma - 1} \sqrt{\frac{\pi k T}{2 m_i}}\, k (T - T_0) \\
&= 1.58 \times 10^{-19} \frac{d\, n\, \alpha}{\gamma - 1} (T - T_0) \sqrt{\frac{T}{M_i}}, \qquad \left[\frac{\mathrm{W}}{\mathrm{cm}}, \mathrm{cm}, \mathrm{cm}^{-3}, \mathrm{K}\right].
\end{aligned} \tag{11}
$$

The power balance

$$p_l = p_b + p_e + p_w$$

gives a third order equation in $\sqrt{T}$:

$$
\begin{aligned}
(T - T_0)\sqrt{T} &= \frac{\gamma - 1}{d\, n\, \alpha\, k^{\frac{3}{2}}} \sqrt{\frac{2 m_i}{\pi}}\, (p_b + p_e + p_w) \\
&= 6.34 \times 10^{18} \frac{\gamma - 1}{d\, n\, \alpha} \sqrt{M_i}\, (p_b + p_e + p_w), \qquad \left[\mathrm{K}, \mathrm{cm}, \mathrm{cm}^{-3}, \frac{\mathrm{W}}{\mathrm{cm}}\right].
\end{aligned} \tag{12}
$$

It is solved numerically. The results are shown in **Figure 5** for both injector types.

4. Gas flow and target thickness

The conductance of a long circular tube (diameter d, length l) in the transition regime may be written (Wutz et al. /13/, p.123) as

$$
\begin{aligned}
C = {} & \frac{\pi}{128} \frac{p\, d^4}{\eta\, l} && \text{(viscous flow)} \\
& + \frac{\pi}{12} \bar{v} \frac{d^3}{l} && \text{(molecular flow, } C_m\text{)} \\
& \times \frac{1 + \sqrt{\frac{8}{\pi}} \frac{p\, d}{\eta\, \bar{v}}}{1 + 1.235 \sqrt{\frac{8}{\pi}} \frac{p\, d}{\eta\, \bar{v}}} && \text{(Knudsen's transition factor),}
\end{aligned}
$$

where η is the viscosity of the gas. This may be rewritten as

$$C = C_m\, k_{tr}$$

with

$$C_m = \frac{\pi}{12} \bar{v} \frac{d^3}{l}$$

and

$$k_{tr} = \frac{1 + \left(\frac{3}{32} + \sqrt{\frac{8}{\pi}}\right)\frac{p\,d}{\eta\,\overline{v}} + \frac{3}{32}\sqrt{\frac{8}{\pi}}\left(\frac{p\,d}{\eta\,\overline{v}}\right)^2}{1 + 1.235\sqrt{\frac{8}{\pi}}\frac{p\,d}{\eta\,\overline{v}}} \tag{14}$$

with $\eta = 0.499\,\rho\,\overline{v}\,\lambda$, the gas density $\rho = m\,n$ and the mean free path $\lambda = 1/(\sqrt{2}\,\pi\,n\,\delta^2)$ (Dushman /14/, p. 28). The molecular diameter for H_2 gas is $\delta = 2.75 \times 10^{-8}$ cm (Dushman, p. 32). With these equations, the transition factor for hydrogen gas becomes

$$k_{tr} = \frac{1 + 4.467 \times 10^{-15} nd + 1.046 \times 10^{-30}(nd)^2}{1 + 5.211 \times 10^{-15} nd} \qquad [\mathrm{cm}^{-3},\ \mathrm{cm}]\,. \tag{14a}$$

The equation for the pV flow

$$q = C(p_1 - p_2)$$

(p_1, p_2 pressures at the ends of the tube) may be transformed into

$$q = \frac{\pi}{12}\,\overline{v}\,d^3 k_{tr}\frac{\mathrm{d}p}{\mathrm{d}z}, \tag{15}$$

where $\mathrm{d}p/\mathrm{d}z$ is the local pressure gradient in the tube. Because

$$\begin{aligned}\frac{\mathrm{d}p}{\mathrm{d}z} &= \frac{\mathrm{d}}{\mathrm{d}z}(nkT)\\ &= kT\left(1 + \frac{n}{T}\frac{\mathrm{d}T}{\mathrm{d}n}\right)\frac{\mathrm{d}n}{\mathrm{d}z},\end{aligned}$$

the variables n and z in the differential equation (15) may be separated into

$$\frac{\pi}{12}\overline{v}\,d^3 k_{tr}\,kT_N\left(1 + \frac{n}{T}\frac{\mathrm{d}T}{\mathrm{d}n}\right)\mathrm{d}n = q_N\,\mathrm{d}z, \tag{16}$$

where the index N means the "normal temperature" for which the usual flow in mbar l/s is given, i.e. $T_N \approx 300$ K. This equation may be integrated once, giving $n = n(q_N z)$

$$\begin{aligned}q_N\,z &= \frac{\pi}{12}\,d^3\,kT_N \int_{n_{end}}^{n} \overline{v}\,[T(n')]\;k_{tr}(n')\left(1 + \frac{n'}{T}\frac{\mathrm{d}T}{\mathrm{d}n'}\right)\mathrm{d}n'\\ &= \sqrt{\frac{\pi k}{18m}}\,d^3\,kT_N \int_{n_{end}}^{n} \sqrt{T(n')}\,k_{tr}(n')\left(1 + \frac{n'}{T}\frac{\mathrm{d}T}{\mathrm{d}n'}\right)\mathrm{d}n'\\ &= 1.54 \times 10^{-16}\frac{d^3}{\sqrt{M}} \int_{n_{end}}^{n} \sqrt{T(n')}\,k_{tr}(n')\left(1 + \frac{n'}{T}\frac{\mathrm{d}T}{\mathrm{d}n'}\right)\mathrm{d}n',\end{aligned} \tag{17}$$

$$\left[\frac{\mathrm{mbar\,l}}{\mathrm{s}},\ \mathrm{cm},\ \mathrm{K},\ \mathrm{cm}^{-3}\right]$$

for $T_N = 293\,\mathrm{K}$, $k_{tr}(n')$ from equation (14), $T(n')$ and $\mathrm{d}T/\mathrm{d}n'$ from the solution of equation (12).

The assumption $n_{end} = 0$ at the open end of the neutralizer gives the dependence $n = n(q_N z)$ as shown in **Figure 6.** It is completely unphysical, however, to assume $n_{end} = 0$. A more reasonable assumption is that at the end of the tube the distribution function of the gas molecules is a one-sided Maxwellian. This implies a very good vacuum in the injector box which prevents any gas from streaming back. On the other hand, beaming of the neutralizer gas is also neglected which would imply a higher average directed velocity of the gas and therefore a lower number density for the same flux. A half-Maxwellian distribution seems to be a good compromise. The particle flux is then

$$\begin{aligned} \dot{N} &= n_{end} \frac{\overline{v}}{2} \frac{\pi}{4} d^2 \\ &= \frac{\pi}{8} d^2 \, n_{end} \, \overline{v} \end{aligned}$$

with

$$\overline{v} = \sqrt{\frac{8kT_0}{\pi m}}.$$

And, because

$$q_N = \dot{N} k T_N,$$

$$\begin{aligned} n_{end} &= \frac{8}{\pi} \frac{1}{\overline{v} d^2} \frac{q_N}{kT_N} \\ &= \sqrt{\frac{8}{\pi}} \frac{1}{d^2} \sqrt{\frac{m}{kT_0}} \frac{q_N}{kT_N}. \end{aligned} \tag{18}$$

From equations (17) and (18) follows

$$\begin{aligned} q_N z &= \sqrt{\frac{\pi k}{18m}} d^3 k T_N \left\{ \int_0^n - \int_0^{n_{end}} \right\} \sqrt{T} \, k_{tr} \left(1 + \frac{n'}{T} \frac{\mathrm{d}T}{\mathrm{d}n'} \right) \mathrm{d}n' \\ &= \sqrt{\frac{\pi k}{18m}} d^3 k T_N \int_0^n \sqrt{T} \, k_{tr} \left(1 + \frac{n'}{T} \frac{\mathrm{d}T}{\mathrm{d}n'} \right) \mathrm{d}n' - \frac{2}{3} d \, q_N, \end{aligned} \tag{19}$$

assuming molecular gas flow in the fictive end part. With the transformation

$$s = q_N \left(z + \frac{2}{3} d \right), \tag{20}$$

equation (19) may be written as

$$\begin{aligned} s &= \sqrt{\frac{\pi k}{18m}} d^3 k T_N \int_0^n \sqrt{T} \, k_{tr} \left(1 + \frac{n'}{T} \frac{\mathrm{d}T}{\mathrm{d}n'} \right) \mathrm{d}n' \\ &= 1.54 \times 10^{-16} \frac{d^3}{\sqrt{M}} \int_0^n \sqrt{T} \, k_{tr} \left(1 + \frac{n'}{T} \frac{\mathrm{d}T}{\mathrm{d}n'} \right) \mathrm{d}n', \left[\frac{\mathrm{mbar\,l}}{\mathrm{s}}, \mathrm{cm}, \mathrm{K}, \mathrm{cm}^{-3} \right], \end{aligned} \tag{21}$$

which gives for molecular flow conditions ($T = T_0$, $k_{tr} = 1$)

$$n = \sqrt{\frac{18m}{\pi k T_0}} \frac{s}{d^3 k T_N}. \tag{22}$$

The equation for the target thickness

$$\Pi = \int_0^l n \, \mathrm{d}z$$

may be transformed with equation (20) into

$$\Pi = \frac{1}{q_N} \int_{q_N \frac{2}{3} d}^{q_N \left(l + \frac{2}{3} d\right)} n(s) \, \mathrm{d}s$$

$$= \frac{1}{q_N} \left[\int_0^{q_N \left(l + \frac{2}{3} d\right)} n \, \mathrm{d}s - \int_0^{q_N \frac{2}{3} d} n \, \mathrm{d}s \right].$$

The second term in the bracket may be integrated using equation (22), giving

$$\Pi_{end} = \frac{2}{3} \sqrt{\frac{2m}{\pi k T_0}} \frac{q_N}{d \, k T_N}$$

$$= 1.44 \times 10^{15} \sqrt{\frac{M}{T_0}} \frac{q_N}{d}, \quad \left[\mathrm{cm}^{-2}, \mathrm{K}, \frac{\mathrm{mbar\,l}}{\mathrm{s}}, \mathrm{cm} \right]. \tag{23}$$

Π_{end} is usually a correction of $\sim 1\%$ to the total Π and can be neglected. The target thickness is thus

$$\Pi = \left(l + \frac{2}{3} d\right) \frac{1}{q_N \left(l + \frac{2}{3} d\right)} \int_0^{q_N \left(l + \frac{2}{3} d\right)} n(s) \, \mathrm{d}s, \tag{24}$$

where the density $n(s)$ is taken from the solution of equation (21).

The local gas density and the target thickness are determined by

1. solving equation (21) which gives a table for $n(s)$ with constant steps in n,
2. generating a second table for $n(s)$ with constant steps in s by interpolating the first table,
3. generating a third table for the integral in equation (24) using the second table,
4. generating a fourth table for $\Pi(q_N)$ according to equation (24) using the third table. This is the interesting result which is then plotted.

For comparison, the target thickness for cold transition flow is also calculated. The same procedure is used. However, in equation (21) the gas temperature is set constant and equal to the neutralizer temperature: $T = T_0$.

The target thickness for molecular flow is also obtained from equations (24) and (21), setting the transition factor $k_{tr} = 1$. In this case, the integral in equation (21) may be easily calculated analytically, and also the integral in equation (24), giving

$$\Pi_{mol} = \sqrt{\frac{9m}{2\pi k T_0}} \frac{q_N \left(l + \frac{2}{3}d\right)^2}{d^3 k T_N}$$

$$= 3.25 \times 10^{15} \sqrt{\frac{M}{T_0}} \frac{q_N \left(l + \frac{2}{3}d\right)^2}{d^3}, \qquad \left[\mathrm{cm}^{-2}, \mathrm{K}, \frac{\mathrm{mbar\,l}}{\mathrm{s}}, \mathrm{cm}\right]. \tag{25}$$

Target thickness versus gas flow is plotted in **Figure 7** for the ASDEX/W7AS injectors and in **Figure 8** for the ASDEX UPGRADE injectors. The figures also show the target thickness as calculated for cold molecular flow and for cold transition flow. The reduction of the target thickness due to beam heating can be seen in both figures. In the case of an ASDEX/W7AS injector the reduction is about 35%, whereas it is about 45% for an ASDEX UPGRADE injector at gas flows of 10 and 30 mbar l/s, respectively.

5. How to keep the neutralizer gas cooler?

One aim of this investigation was to look for a method to increase the target thickness for fixed neutralizer geometry and gas flux. We must therefore know how much each heating process contributes. Direct heating by the beam cannot be avoided. So we may take this heating power as a basis for comparison. Heating by ion reflection at the wall relating to beam heating is shown in **Figure 9** for standard parameters. This ratio is rather independent of the gas density and mainly depends on the electron temperature and the reflection factor. If the reflection factor could be reduced to nearly zero, we could at best save a heating power of the order of the direct beam heating power. **Figure 10** shows the ratio of gas heating by electrons to direct heating by the beam, also for standard parameters. Electron heating is higher than beam heating only at higher densities. If we had the possibility of cooling down the electron gas, we would again save a power of the order of the direct heating power.

The dependence of the target thickness on parameter variations is studied in **Figures 11** and **12** where the target thicknesses increase from step to step for a given gas flux. Curve 1 is the reference curve for "standard" parameters. For curve 2 the wall reflection of ions is reduced, for curve 3 additionally the wall accommodation is increased. In case 4 the average energy E_s with which secondary electrons are created is arbitrarily reduced to a low value to simulate electron cooling. In case 5, finally, the neutralizer is additionally cooled down to about liquid nitrogen temperature.

To realize such parameter variations involves difficulties of various degrees. The simplest method is certainly to make the neutralizer surface very rough and structured so that ions are not reflected into the gas and temperature accommodation of the hot gas is improved.

The most difficult method may be to cool down the electron gas because large-area cathodes are needed to effectively decrease the electron-confining space-charge sheath at the walls. Cooling down the neutralizer to LN_2 temperature, on the other hand requires much less effort than installing cryo pumps in an injector.

It is therefore *proposed to investigate* on a test bed

– the effect of a *rough surface structure* and

– the effect of *neutralizer cooling*

on the gas target thickness.

It is well known within the neutral beam community that the angular distribution of the ion beam may be represented by the sum of a Gaussian (with a $(1/e)$-divergence of 0.5–2°) and a very broad halo containing of the order of 20% of the beam power. This halo gives a higher power load to the neutralizer surface in the vicinity of the ion source. It may be advisable therefore to divide the neutralizer into two parts and cool down only the downstream end.

6. Scaling considerations

The simple equation (25) for molecular flow is the main guideline for cold gas flow in the neutralizer. The transition-flow correction is relatively small. The dependence of the cold target thickness on several parameters is therefore essentially

$$\Pi_{cold} \propto \frac{q_N\, l^2}{T_0^{0.5}\, d^3}. \tag{26}$$

It will be interesting to investigate the parameter dependences also of the hot target thickness. This is done using a series of log-log plots (**Figures 13 - 17**) varying only one parameter and keeping the other parameters at "standard" values. These figures give the scaling

$$\Pi_{hot} \propto \frac{q_N^{0.8}\, l^{1.6-1.7}}{T_0^{0.1-0.2}\, d^{2.2-2.3}\, I^{0.2}}. \tag{27}$$

The dependences on length and diameter are still strong, and it has to be emphasized that a neutralizer should be built not only as long as possible but also as narrow as possible. The wall temperature T_0 has got a very weak dependence. Cooling the neutralizer to liquid nitrogen temperature would bring nearly no advantage. It would make sense only in combination with an improved wall accomodation and a decreased ion reflectivity. The beam current has also an effect, however weak.

7. What is the cause for the enhanced emission of unshifted H_α radiation?

This investigation was triggered by the suspicion that a very hot electron gas produces H_α emission in collisions with H_2 molecules. It has been shown above that the electrons are not that energetic and probably have a temperature of less than just 4 eV. Janev (/10/, p. 51) gives a reaction rate for the process

$$e + H_2 \rightarrow e + H + H^*(n = 3)$$

which is $< 10^{-11}\,\mathrm{cm}^3/\mathrm{s}$ for this electron temperature and is thus too small for the process to play any role. There are other candidates, however: dissociative recombination of H_2^+ or H_3^+.

Tawara /11/ gives a cross-section for the process

$$e + H_2^+ \rightarrow H^0(1s) + H^0(n = 3)$$

which may be approximated by

$$\sigma = \sigma_0 \frac{E_0}{E}$$

with $\sigma_0 = 10^{-15}\,\mathrm{cm}^2$ and $E_0 = 1\,\mathrm{eV}$. This cross-section gives a Maxwellian rate coefficient of

$$\langle \sigma v \rangle = \frac{6.7 \times 10^{-8}}{\sqrt{T_e}} \qquad \left[\frac{\mathrm{cm}^3}{\mathrm{s}}, \mathrm{eV}\right].$$

We may thus calculate the unshifted line intensity caused by the beam and plasma together (as we would measure it) and compare it with the intensity caused by the beam alone. The ratio is shown in **Figure 18**, which, for $n = 10^{14}\,\mathrm{cm}^{-3}$, gives an enhancement by a factor of 4 for an ASDEX/W7AS injector. Although this factor is still a little low compared with the experiment, we may be near the truth with this explanation—keeping in mind that a real beam also contains molecules and their breakup products, which may enhance the plasma density and the correlated light emission.

Appendix I: Coulomb beam heating of the neutralizer plasma by the beam

The energy loss of a monoenergetic beam due to the interaction with plasma electrons and ions is treated by Sivukhin (equations (8.1) and (8.2) of /15/). His equations may be rewritten into the form given in the NRL Plasma Formulary /16/. This gives the energy loss of the beam

$$\left\langle \frac{\mathrm{d}E_b}{\mathrm{d}t} \right\rangle = -\frac{4\pi e^4 \lambda_{ie}\, n_t}{(4\pi\epsilon_0)^2\, v_b\, m_t} \left[\mathrm{M}(x_\beta) - \frac{m_t}{m_b} \mathrm{M}'(x_\beta) \right] \tag{AI-1}$$

with

E_b = beam energy

λ_{ie} = Coulomb logarithm

v_b = beam velocity

m_t = mass of target particles

m_b = mass of beam particles

$$\mathrm{M}(x_\beta) = \frac{2}{\sqrt{\pi}} \int_0^{x_\beta} \sqrt{t} \exp(-t)\,\mathrm{d}t$$

$$x_\beta = \frac{m_t}{m_b} \frac{E_b}{T_t}$$

T_t = temperature of the target particles.

The term containing M′ may be neglected because for both ions and electrons

$$(m_t/m_b)\,\mathrm{M}'(x_\beta) \ll \mathrm{M}(x_\beta).$$

The Coulomb logarithm may be set to

$$\lambda_{ie} = 15,$$

and, in the numerical evaluation, the fit is used

$$\mathrm{M}(x_\beta) = 1 - \exp\left(-0.5453\, x_\beta^{1.2989}\right).$$

The energy gain of the target particles per unit length is

$$\begin{aligned} h_{bt} &= \frac{\pi}{4} d^2\, n_b \left\langle -\frac{\mathrm{d}E_b}{\mathrm{d}t} \right\rangle \\ &= \frac{2\pi e^3 \lambda_{ie}\, \mathrm{M}(x_\beta)\, \xi\, I_b}{(4\pi\epsilon_0)^2\, E_b} \frac{m_b}{m_t}. \end{aligned} \tag{AI-2}$$

This heating power is small for electrons as target particles and even much smaller (by the electron/ion mass ratio) for the ions. Nevertheless, equation (AI-2) is included in the electron energy balance of equation (5).

Appendix II: Cross section σ_{ib}

There are three processes involved in the formation of H_2^+-ions in the neutralizer by beam-gas collisions:

1. $\underline{H^+} + H_2 \rightarrow \underline{H^+} + H_2^+ + e$
2. $\underline{H^+} + H_2 \rightarrow \underline{H^0} + H_2^+$
3. $\underline{H^0} + H_2 \rightarrow \underline{H^0} + H_2^+ + e.$

Taking

$\sigma_1 = 2.2 \times 10^{-16}\,\mathrm{cm}^2$ Solov'ev /17/

$\sigma_2 = 1.6 \times 10^{-16}\,\mathrm{cm}^2$ Massey and Gilbody /18/

$\sigma_3 = 1.4 \times 10^{-16}\,\mathrm{cm}^2$ Solov'ev /17/

for the three processes, respectively, and an average charge fraction of $\xi = 0.7$ (in accordance with Paméla), gives an average cross-section for H_2^+-production

$$\begin{aligned}\sigma_{ib} &= (\sigma_1 + \sigma_2)\xi + \sigma_3(1-\xi) \\ &= 3.1 \times 10^{-16}\mathrm{cm}^2.\end{aligned}$$

Appendix III: ASDEX UPGRADE Neutralizers

The neutralizers for the ASDEX UPGRADE injectors have a complicated shape. Their cross section varies along the whole length. The upper and lower walls are plane whereas the side walls are circular. The shape is indicated in **Figure 19** which explains the meaning of the cross section parameters a, b and r.

The Knudsen relation (Dushman /14/, p. 87)

$$Q = \frac{4}{3} \frac{\overline{v}\,(p_1 - p_2)}{\int_0^l \frac{H}{A^2}\,\mathrm{d}l}$$

(H = circumference, A = area) is used to calculate the effective diameter of a circular tube which has the same conductivity

$$d_{eff} = \left(\frac{16}{\pi} \frac{A^2}{H} \right)^{\frac{1}{3}} .$$

The following table gives the values of a, b and r at the distance z from the ion source and the calculated d_{eff} (all dimensions in mm)

#	z	a	b	r	d_{eff}
1	0	62	231	226	362.8
2	818	62	266	226	391.2
3	818	0	280	258	403.2
4	1001	0	260	245	378.5
5	1001	0	544	272	544.0
6	1182	0	544	272	544.0
7	1182	0	280	255	401.0
8	2000	0	200	220	312.8

The calculated values of d_{eff} are used in the figure to indicate the shape of the neutralizers. The diameter used for a cylindrical tube simulating this complicated shape was $d = 357.4$ mm. This simulation tube is also indicated in the figure.

REFERENCES

1. J. Paméla, *Gas heating effects in the neutralisers of neutral beam injection lines*, Laboratory Report, EUR-CEA-FC-1279, CEN-Fontenay-aux-Roses, France, September 1985.
2. J. Paméla, Rev. Sci. Instr. **57** (1986), p. 1066.
3. I.D. Williams, J. Geddes and H.B. Gilbody, *I*, J. Phys. B: At. Mol. Phys. **15** (1982), p. 1377; *II*, J. Phys. B: At. Mol. Phys. **16** (1983), p. L765.
4. D.B. Heifetz et al., *H_α studies on TFTR*, Laboratory Report PPPL-2541, Plasma Physics Laboratory, Princeton University, Princeton, N.J. 08543, USA, August 1988.
5. D.K. Gibson and I.D. Reid, *Double differential cross sections for electrons ejected from H_2 and other gases by 50 keV protons*, Laboratory Report AAEC/E659, Australian Atomic Energy Commission, Research Establishment, Lucas Heights Research Laboratories, April 1987.
6. D.K. Gibson, Australian Nuclear Science & Technology Organisation, private communication, February 1988.
7. D. Bohm, "The characteristics of electrical discharges in magnetic fields", McGraw-Hill, New York, 1949, p. 77.
8. J.T. Scheuer and G.A. Emmert, *Sheath and presheath in a collisionless plasma with a Maxwellian source*, Laboratory Report, Nuclear Engineering and Physics Department, Univ. of Wisconsin, Madison, WI 53706-1687, January 1988.
9. W. Ott, Z. Naturforschung **17a** (1962), p. 962.
10. R. K. Janev, W. D. Langer, K. Evans and D. E. Post, "Elementary processes in hydrogen-helium plasmas, cross-sections and reaction rate coefficients", Springer Verlag, Berlin, Heidelberg, 1987.
11. H. Tawara et al., *Atomic data involving hydrogens relevant to edge plasmas*, Laboratory Report IPPJ-AM-46, Institute of Plasma Physics, Nagoya University, Nagoya, Japan, July 1986.
12. W. Eckstein, Appl. Phys. **A38** (1985), p. 123.
13. M. Wutz, H. Adam and W. Walcher, "Theorie und Praxis der Vakuumtechnik", Vieweg Verlag, Braunschweig, Germany, 3rd ed., 1986.
14. S. Dushman and J.M. Lafferty, "Scientific foundations of vacuum technique", John Wiley & Sons, New York, London, 2nd ed., 1962.
15. D.V.Sivukhin, *Coulomb collisions in a fully ionized plasma*, "Reviews of Plasma Physics", edited by M.A.Leontovich, English translation, Consultants Bureau, New York, USA, 1966, p. 93-241.
16. D.L. Book and A.W.Ali, *A collection of plasma physics formulas and data*, NRL Memorandum Report 2898, January 1975, Naval Research Laboratory, Washington, D.C., USA.
17. E.S. Solov'ev, R.N. Il'in, V.A. Oparin and N.V. Fedorenko, J. Exptl. Theoret. Phys. (USSR) **42** (1962), p. 659.
18. H.S.W. Massey and H.B. Gilbody, "Electronic and ionic impact phenomena, Vol IV: Recombination and fast collisions with heavy particles", Clarendon Press, Oxford, 1974.

List of symbols

C	gas flow conductance
C_m	conductance in the molecular flow regime
d	neutralizer diameter
E_b	beam energy
E_d	average energy loss of electrons in dissociating collisions with H_2
$\langle E_{H^0,b} \rangle$	average energy of H^0 atoms generated from H_2 in collisions with beam protons
$\langle E_{H^+,b} \rangle$	average energy of H^+ ions generated from H_2 in collisions with beam protons
$\langle E_{H^0,e} \rangle$	average energy of H^0 atoms generated from H_2 in collisions with electrons
E_i	ionization energy of H_2
E_s	average initial energy of electrons created in beam gas collisions
f_{tr}^0	fraction of energy transferred from several-*eV* *neutral* particles to hydrogen gas
f_{tr}^+	fraction of energy transferred from several-*eV* *charged* particles to hydrogen gas
I_b	beam current
j_i	ion current to the wall
k	Boltzmann constant
k_{tr}	transition factor for the gas flow
l	neutralizer length
m_e	electron mass
m_i	ion mass
M_i	ion mass number corresponding to m_i
$\mathrm{M}(x_\beta)$	see Appendix I
n	H_2 gas density
n_b	density of beam ions
n_e	electron density
n_{end}	gas density at the open end of the neutralizer
n_{es}	electron density obtained by the simple balance (7b)
$\dot{N}$	flux of gas particles through the neutralizer
p	gas pressure
p_b	power per unit length of the neutralizer transferred from the *beam* to the gas
p_e	power transferred from the *electrons*
p_l	power *lost* by the gas to the wall
p_w	power transferred from the *ions reflected from the wall*
q	$p \times V$ gas flow through neutralizer
q_N	$p \times V$ gas flow for $T = T_N$
r_w	energy reflection coefficient for ions hitting the neutralizer wall
s	integration variable, $= q_N \left(z + \frac{2}{3}d\right)$

T	gas temperature
T_e	electron temperature
T_{es}	electron temperature obtained by the simple balance (7a)
T_N	normal temperature of the surroundings, $T_N \sim 300\,\mathrm{K}$
T_0	temperature of the neutralizer wall
U_f	floating potential of the wall with respect to the axis
$\overline{v}$	average gas velocity
z	distance from the open end of the neutralizer
α	accomodation factor for the gas hitting the neutralizer wall
γ	specific heat ratio
η	gas viscosity
λ_{ie}	see Appendix I
Π	gas target thickness
σ_{H^0}	cross section for generation of H^0 atoms in proton collisions with H_2 molecules
σ_{H^+}	cross section for generation of H^+ ions in proton collisions with H_2 molecules
σ_i	cross section for H_2^+ formation in electron collisions with H_2 molecules
$\langle \sigma_i v_e \rangle$	corresponding rate coefficient
σ_{ib}	cross section for H_2^+ formation in proton collisions with H_2 molecules
σ_{tr}^0	elastic-collision cross-section for several-eV *neutral* particles with hydrogen molecules
σ_{tr}^+	elastic-collision cross-section for several-eV *charged* particles with hydrogen molecules
τ	confinement time of ions and electrons
ξ	average charge fraction of beam

Additional symbols used only once are explained in their context.

Figure Captions

Figure 1: H_α spectra from neutralizer and target tank
Figure 2: Electron density versus neutral gas density for W7AS injectors
Figure 3: Electron density versus neutral gas density for ASDEX UPGRADE injectors
Figure 4: Electron temperature versus neutral gas density
Figure 5: Gas temperature versus gas density
Figure 6: Gas density versus product gas flux $\times$ distance
Figure 7: Target thickness versus gas flow for W7AS injectors
Figure 8: Target thickness versus gas flow for ASDEX UPGRADE injectors
Figure 9: Heating ratio of wall reflection to beam versus gas density
Figure 10: Heating ratio of electrons to beam
Figure 11: Target thickness versus gas flow, parameter study, W7AS injectors
Figure 12: Target thickness versus gas flow, parameter study, ASDEX UPGRADE injectors
Figure 13: Scaling of target thickness with gas flow
Figure 14: Scaling of target thickness with neutralizer length
Figure 15: Scaling of target thickness with neutralizer temperature
Figure 16: Scaling of target thickness with neutralizer diameter
Figure 17: Scaling of target thickness with beam current
Figure 18: Unshifted H_α: Ratio of the emission caused by electrons and beam together to the emission caused by the beam alone
Figure 19: Cross section of the neutralizers for the ASDEX UPGRADE injectors

Fig. 1 H_α-Spectroscopy

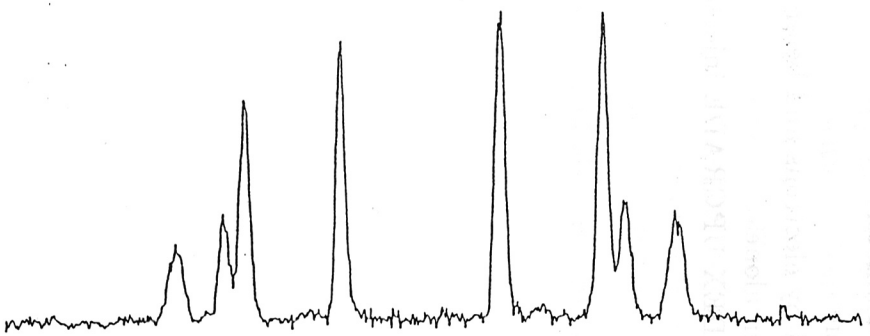

E_0 $\frac{E_0}{2}$ $\frac{E_0}{3}$ λ_0 λ_0 $\frac{E_0}{3}$ $\frac{E_0}{2}$ E_0

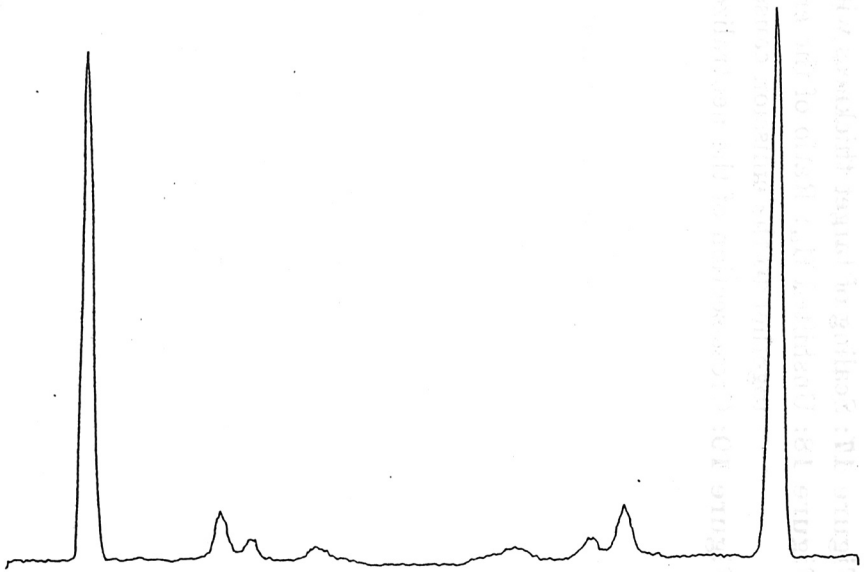

λ_0 $\frac{E_0}{3}$ $\frac{E_0}{2}$ E_0 E_0 $\frac{E_0}{2}$ $\frac{E_0}{3}$ λ_0

in the target tank:

$$\frac{I_{unshifted}}{\sum I_{shifted}} \approx \frac{1}{2}$$

as expected according to Williams

in the neutralizer:

$$\frac{I_{unshifted}}{\sum I_{shifted}} \gg 1$$

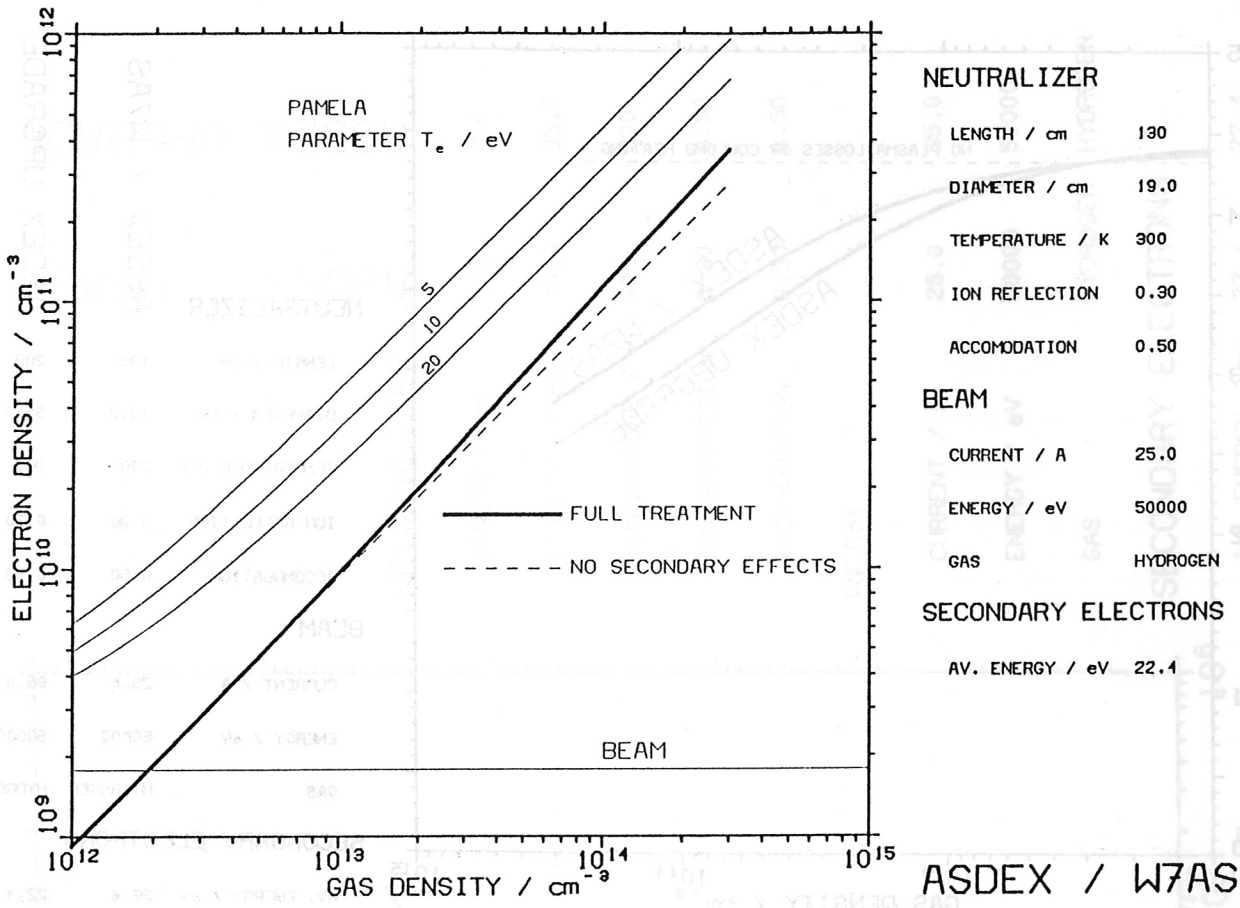
PAMELA
PARAMETER T_e / eV
5
10
20
FULL TREATMENT
NO SECONDARY EFFECTS
BEAM
ELECTRON DENSITY / cm^{-3}
GAS DENSITY / cm^{-3}
10^{12}
10^{11}
10^{10}
10^{9}
10^{13}
10^{14}
10^{15}
NEUTRALIZER
LENGTH / cm 130
DIAMETER / cm 19.0
TEMPERATURE / K 300
ION REFLECTION 0.30
ACCOMODATION 0.50
BEAM
CURRENT / A 25.0
ENERGY / eV 50000
GAS HYDROGEN
SECONDARY ELECTRONS
AV. ENERGY / eV 22.4
ASDEX / W7AS

Fig. 2

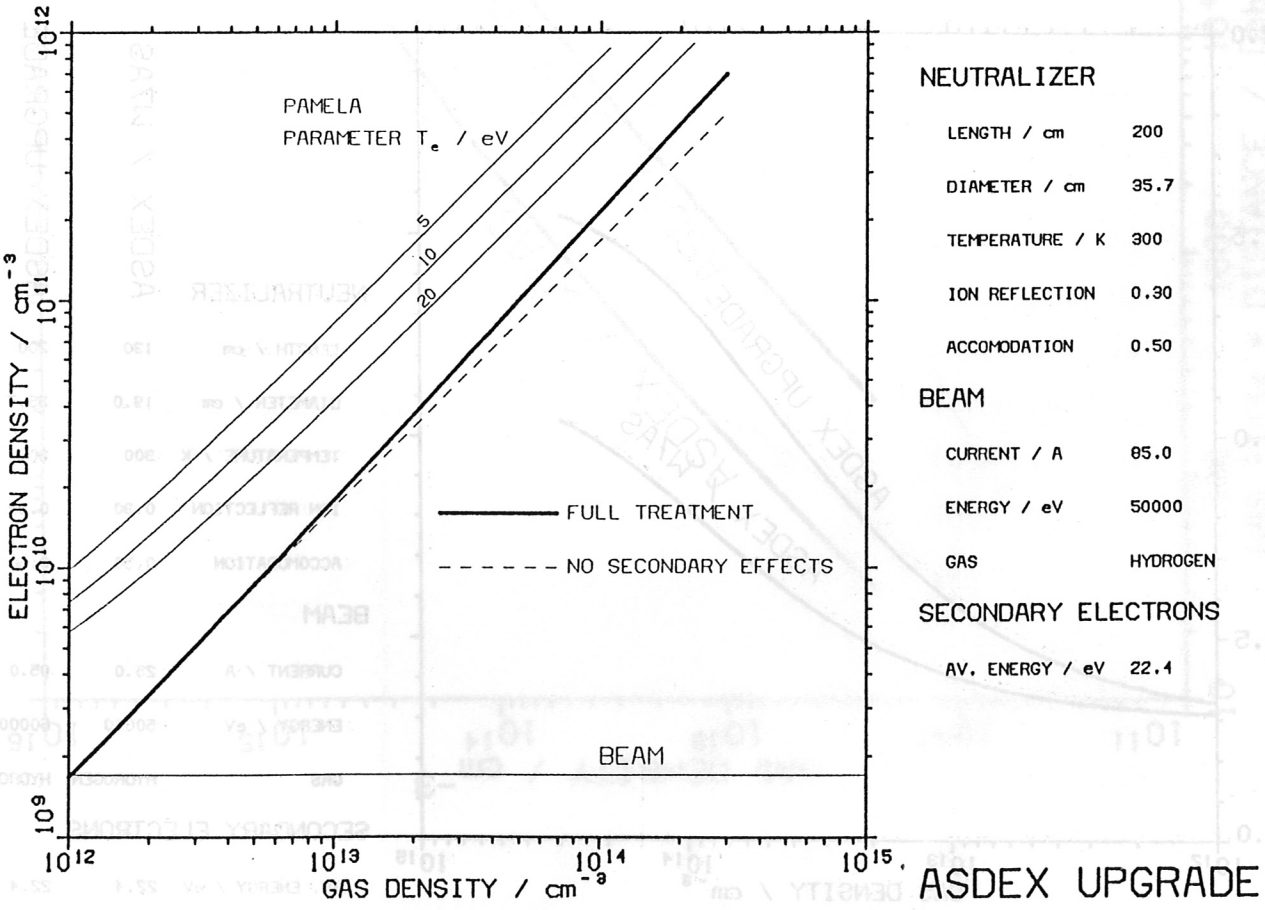
PAMELA
PARAMETER T_e / eV
5
10
20
FULL TREATMENT
NO SECONDARY EFFECTS
BEAM
ELECTRON DENSITY / cm^{-3}
GAS DENSITY / cm^{-3}
10^{12}
10^{11}
10^{10}
10^{9}
10^{13}
10^{14}
10^{15}
NEUTRALIZER
LENGTH / cm 200
DIAMETER / cm 35.7
TEMPERATURE / K 300
ION REFLECTION 0.30
ACCOMODATION 0.50
BEAM
CURRENT / A 65.0
ENERGY / eV 50000
GAS HYDROGEN
SECONDARY ELECTRONS
AV. ENERGY / eV 22.4
ASDEX UPGRADE

Fig. 3

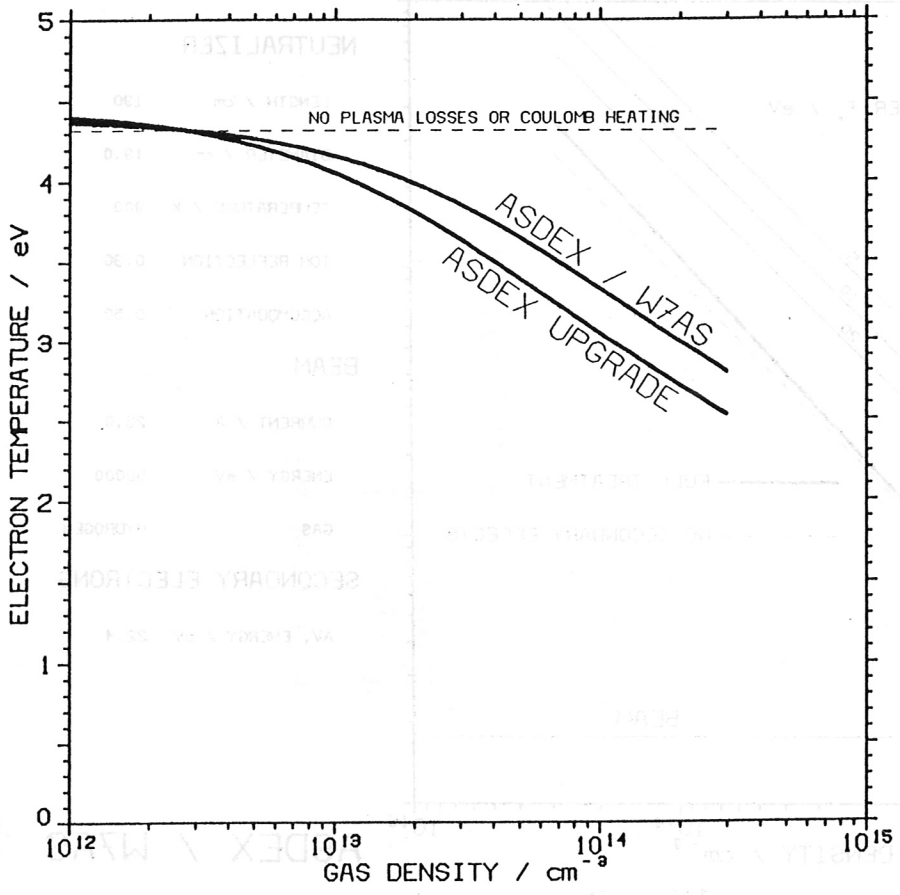

	ASDEX / W7AS	ASDEX UPGRADE
NEUTRALIZER		
LENGTH / cm	130	200
DIAMETER / cm	19.0	35.7
TEMPERATURE / K	300	300
ION REFLECTION	0.30	0.30
ACCOMODATION	0.50	0.50
BEAM		
CURRENT / A	25.0	65.0
ENERGY / eV	50000	50000
GAS	HYDROGEN	HYDROGEN
SECONDARY ELECTRONS		
AV. ENERGY / eV	22.4	22.4

Fig. 4

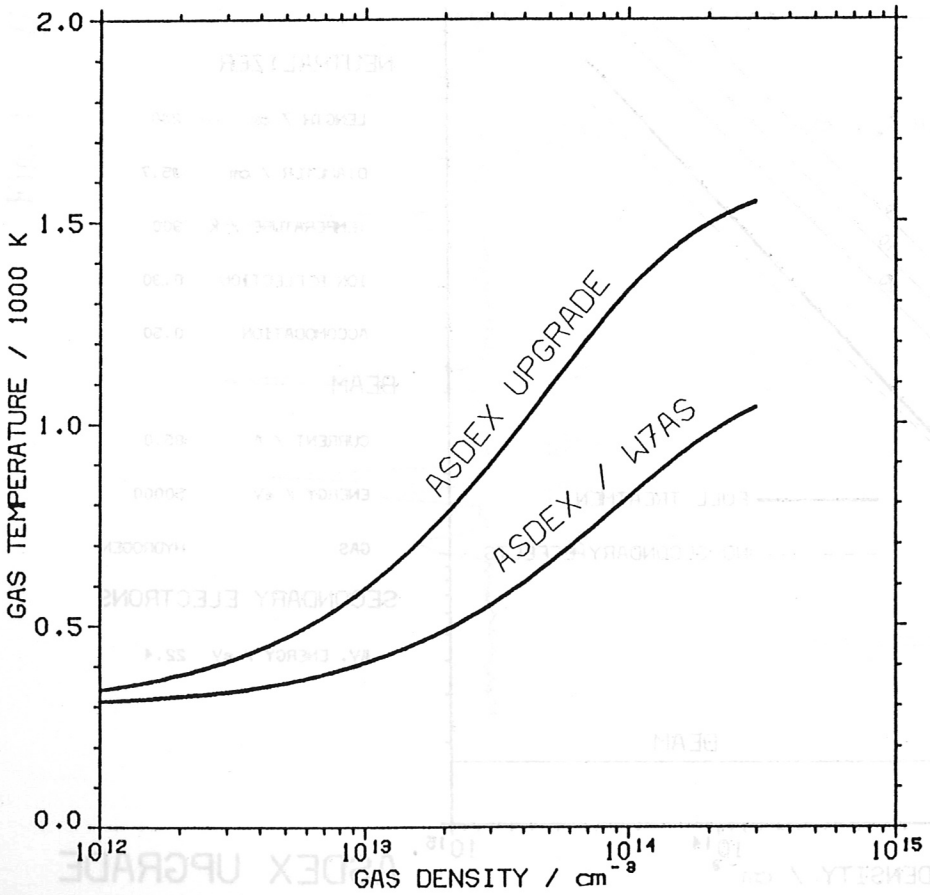

	ASDEX / W7AS	ASDEX UPGRADE
NEUTRALIZER		
LENGTH / cm	130	200
DIAMETER / cm	19.0	35.7
TEMPERATURE / K	300	300
ION REFLECTION	0.30	0.30
ACCOMODATION	0.50	0.50
BEAM		
CURRENT / A	25.0	65.0
ENERGY / eV	50000	50000
GAS	HYDROGEN	HYDROGEN
SECONDARY ELECTRONS		
AV. ENERGY / eV	22.4	22.4

Fig. 5

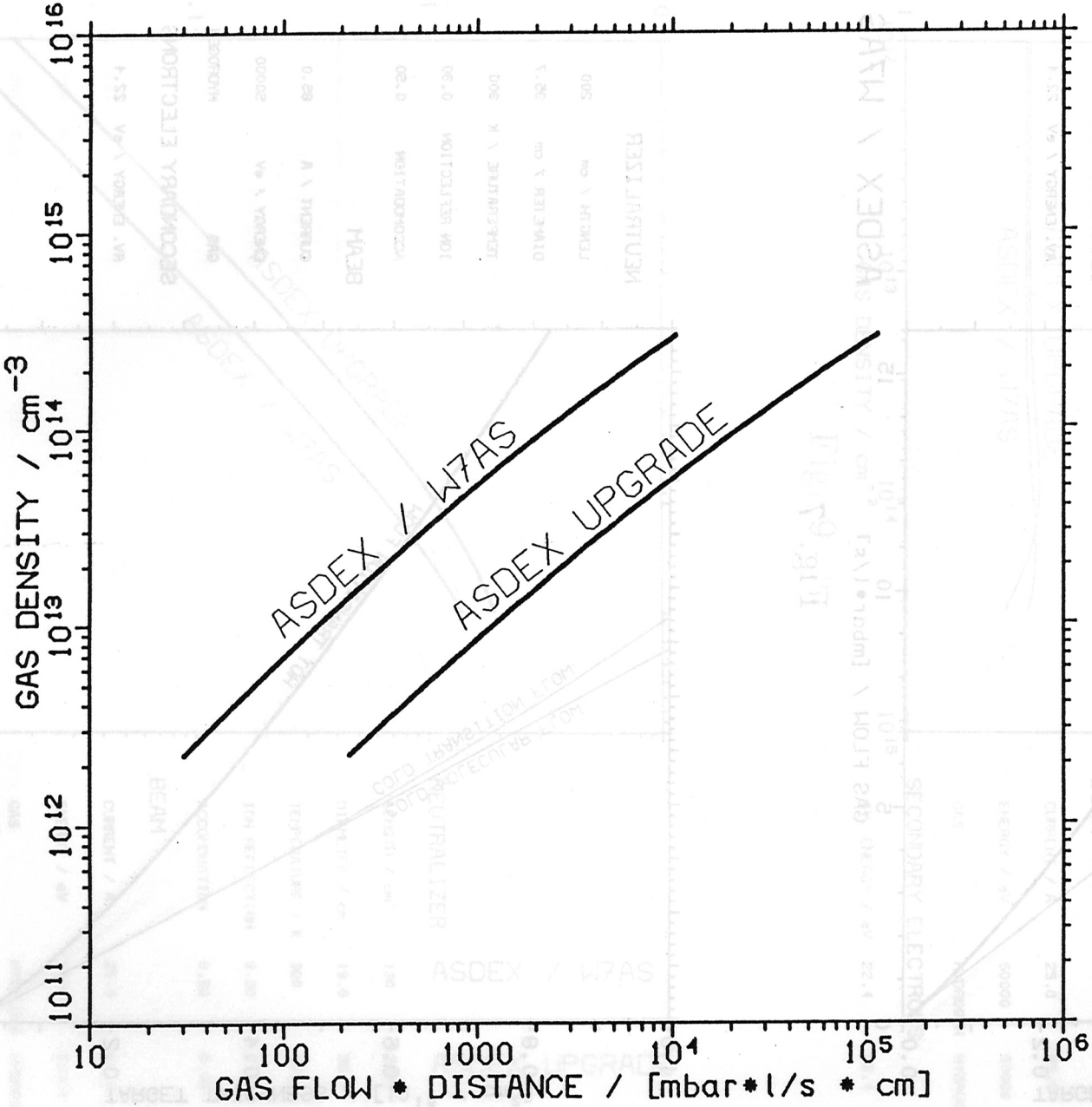

	ASDEX / W7AS	ASDEX UPGRADE
NEUTRALIZER		
LENGTH / cm	130	200
DIAMETER / cm	19.0	35.7
TEMPERATURE / K	300	300
ION REFLECTION	0.30	0.30
ACCOMODATION	0.50	0.50
BEAM		
CURRENT / A	25.0	85.0
ENERGY / eV	50000	50000
GAS	HYDROGEN	HYDROGEN
SECONDARY ELECTRONS		
AV. ENERGY / eV	22.4	22.4

Fig. 6

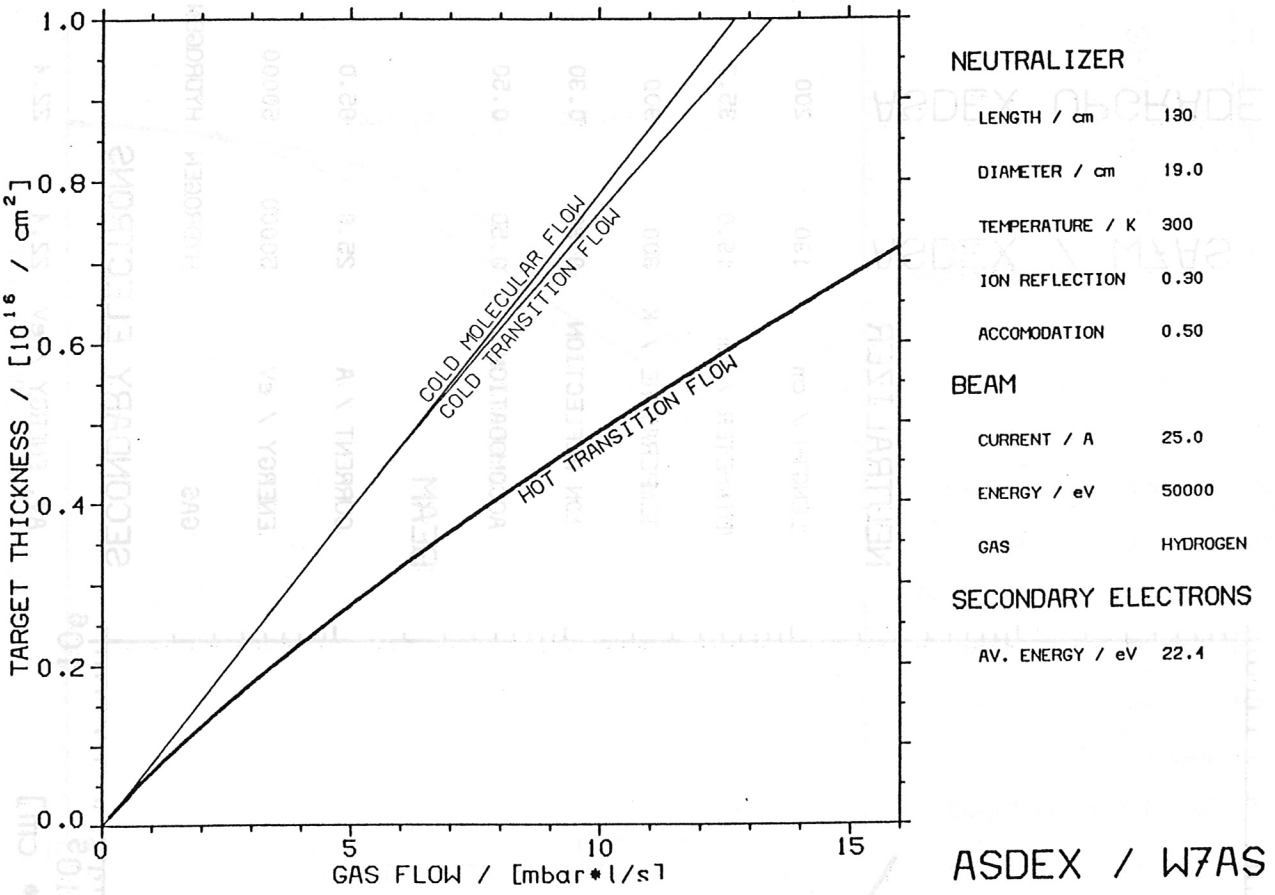
TARGET THICKNESS / [10^16 / cm^2]
GAS FLOW / [mbar*l/s]
COLD MOLECULAR FLOW
COLD TRANSITION FLOW
HOT TRANSITION FLOW
NEUTRALIZER
LENGTH / cm 130
DIAMETER / cm 19.0
TEMPERATURE / K 300
ION REFLECTION 0.30
ACCOMODATION 0.50
BEAM
CURRENT / A 25.0
ENERGY / eV 50000
GAS HYDROGEN
SECONDARY ELECTRONS
AV. ENERGY / eV 22.4
ASDEX / W7AS

Fig. 7

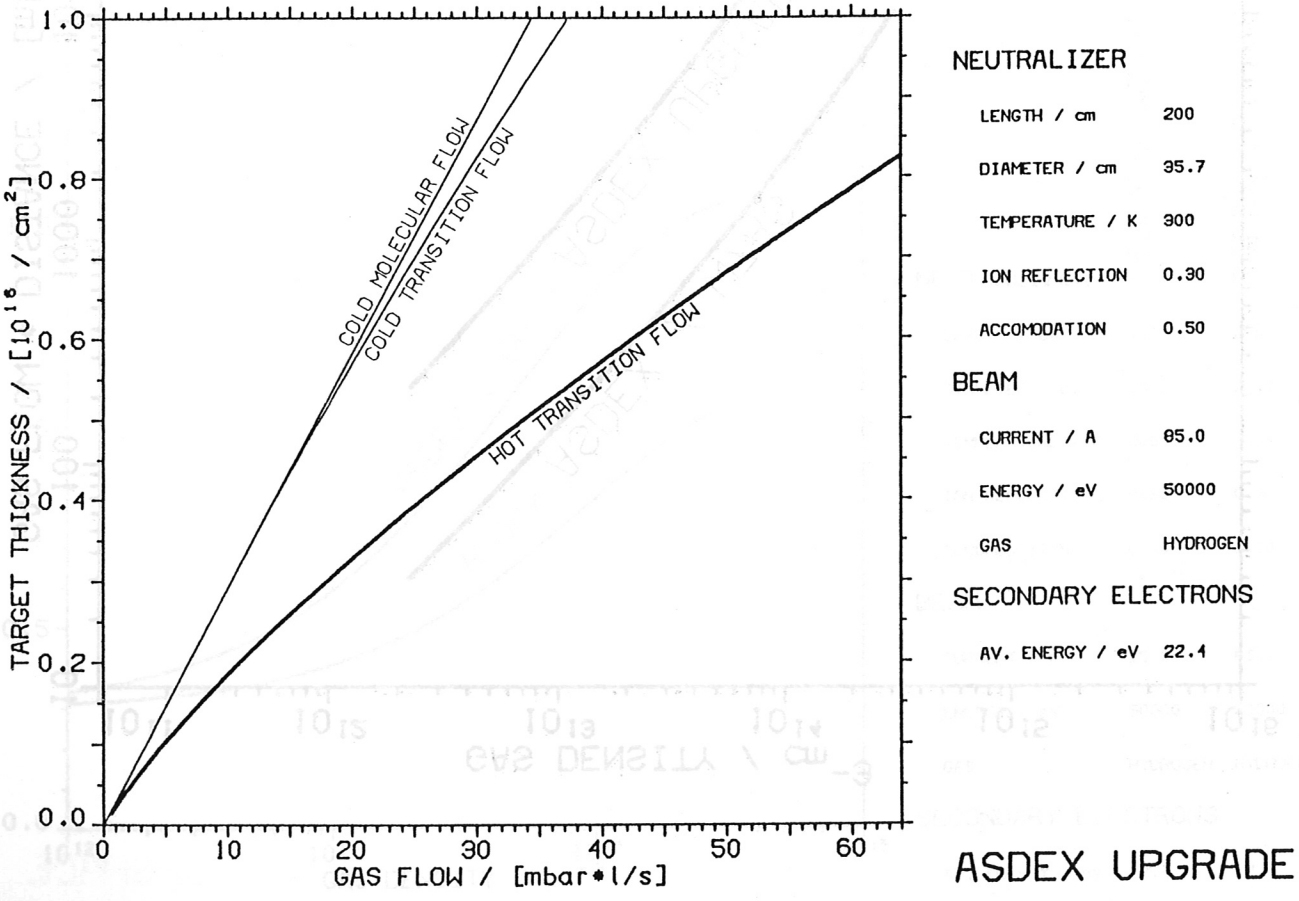
TARGET THICKNESS / [10^16 / cm^2]
GAS FLOW / [mbar*l/s]
COLD MOLECULAR FLOW
COLD TRANSITION FLOW
HOT TRANSITION FLOW
NEUTRALIZER
LENGTH / cm 200
DIAMETER / cm 35.7
TEMPERATURE / K 300
ION REFLECTION 0.30
ACCOMODATION 0.50
BEAM
CURRENT / A 65.0
ENERGY / eV 50000
GAS HYDROGEN
SECONDARY ELECTRONS
AV. ENERGY / eV 22.4
ASDEX UPGRADE

Fig. 8

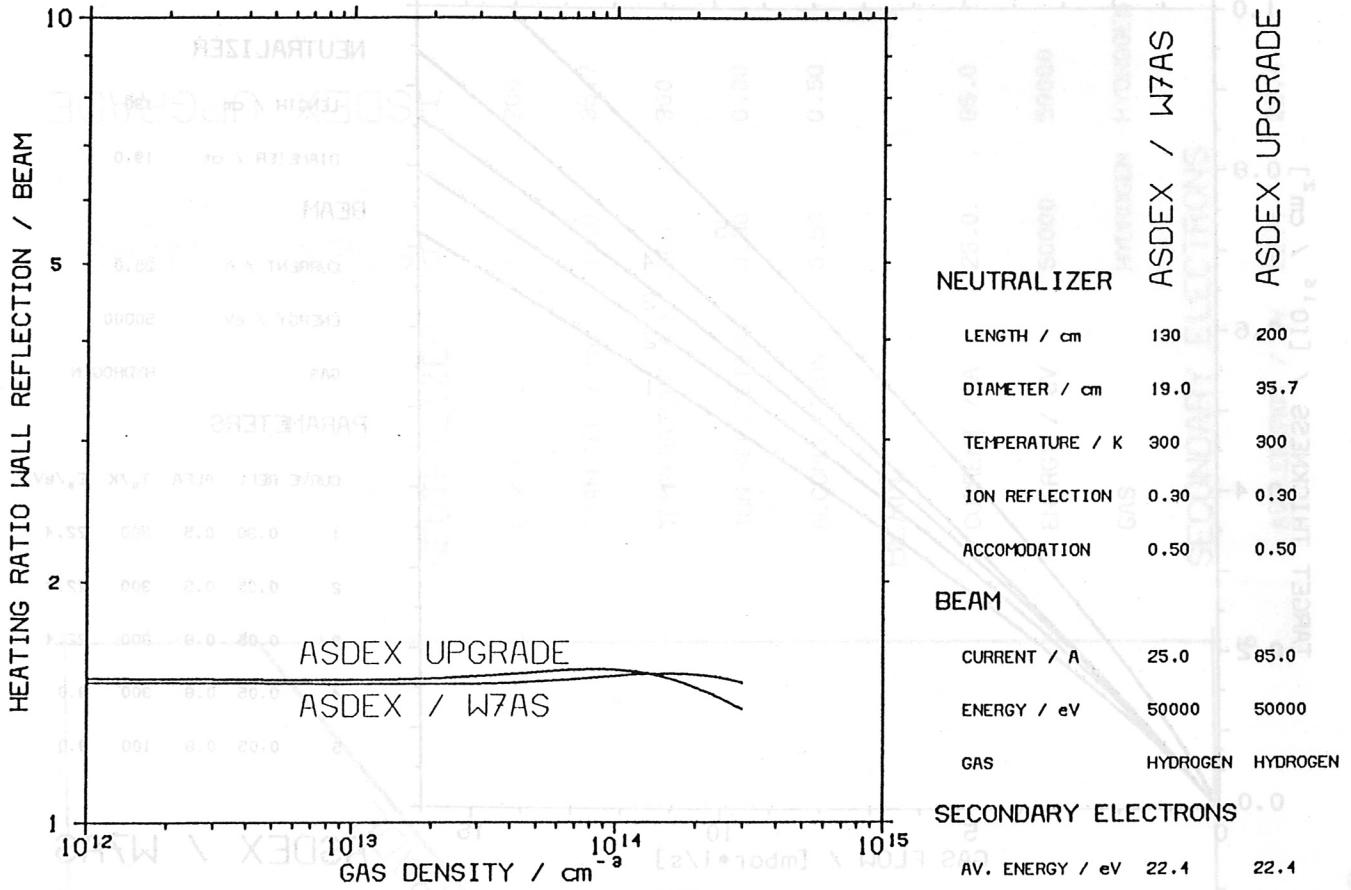
HEATING RATIO WALL REFLECTION / BEAM
10
5
2
1
ASDEX UPGRADE
ASDEX / W7AS
10^{12}
10^{13}
10^{14}
10^{15}
GAS DENSITY / cm^{-3}
ASDEX / W7AS
ASDEX UPGRADE
NEUTRALIZER
LENGTH / cm 130 200
DIAMETER / cm 19.0 35.7
TEMPERATURE / K 300 300
ION REFLECTION 0.30 0.30
ACCOMODATION 0.50 0.50
BEAM
CURRENT / A 25.0 85.0
ENERGY / eV 50000 50000
GAS HYDROGEN HYDROGEN
SECONDARY ELECTRONS
AV. ENERGY / eV 22.4 22.4

Fig. 9

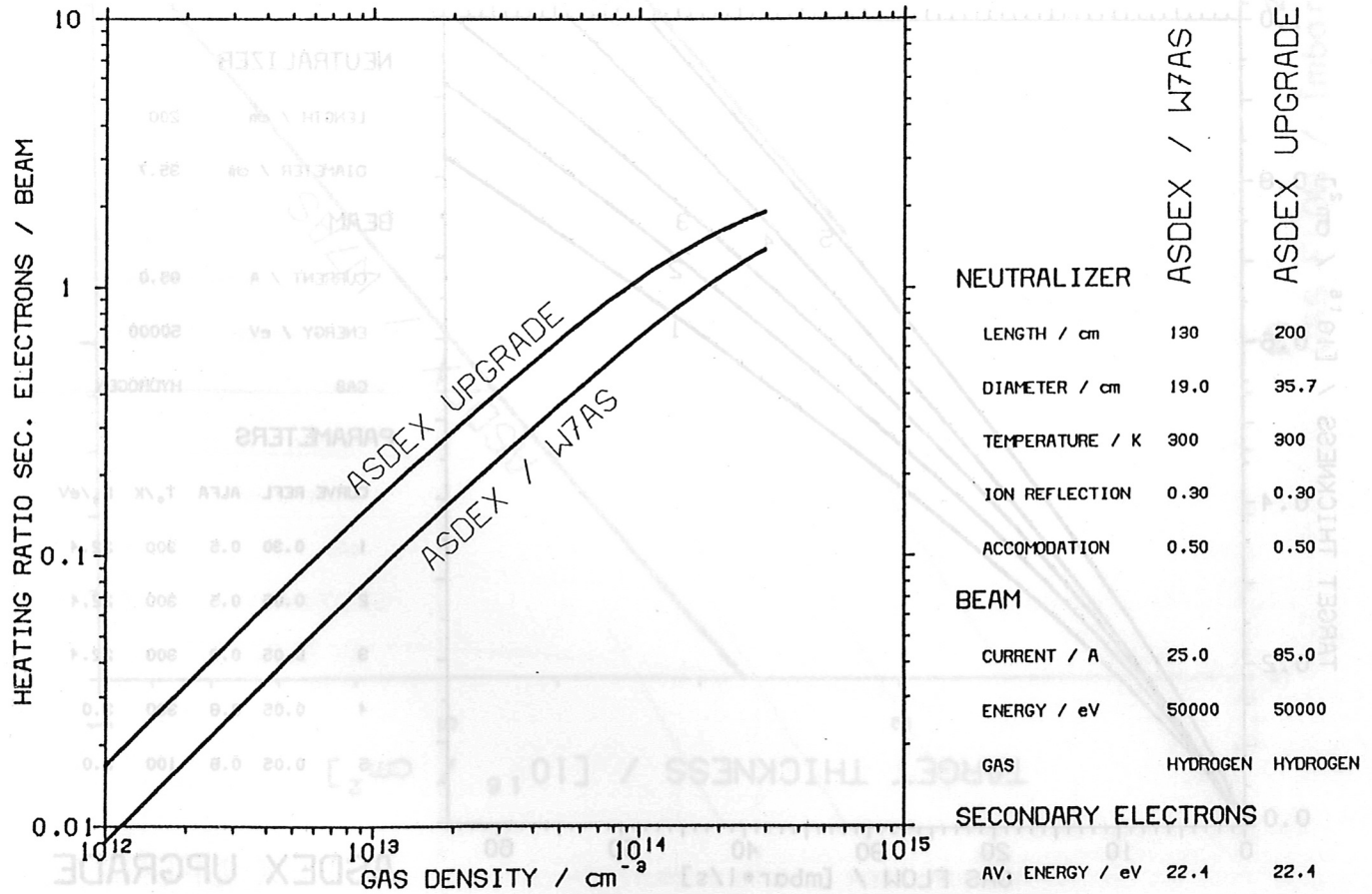
HEATING RATIO SEC. ELECTRONS / BEAM
10
1
0.1
0.01
ASDEX UPGRADE
ASDEX / W7AS
10^{12}
10^{13}
10^{14}
10^{15}
GAS DENSITY / cm^{-3}
ASDEX / W7AS
ASDEX UPGRADE
NEUTRALIZER
LENGTH / cm 130 200
DIAMETER / cm 19.0 35.7
TEMPERATURE / K 300 300
ION REFLECTION 0.30 0.30
ACCOMODATION 0.50 0.50
BEAM
CURRENT / A 25.0 85.0
ENERGY / eV 50000 50000
GAS HYDROGEN HYDROGEN
SECONDARY ELECTRONS
AV. ENERGY / eV 22.4 22.4

Fig. 10

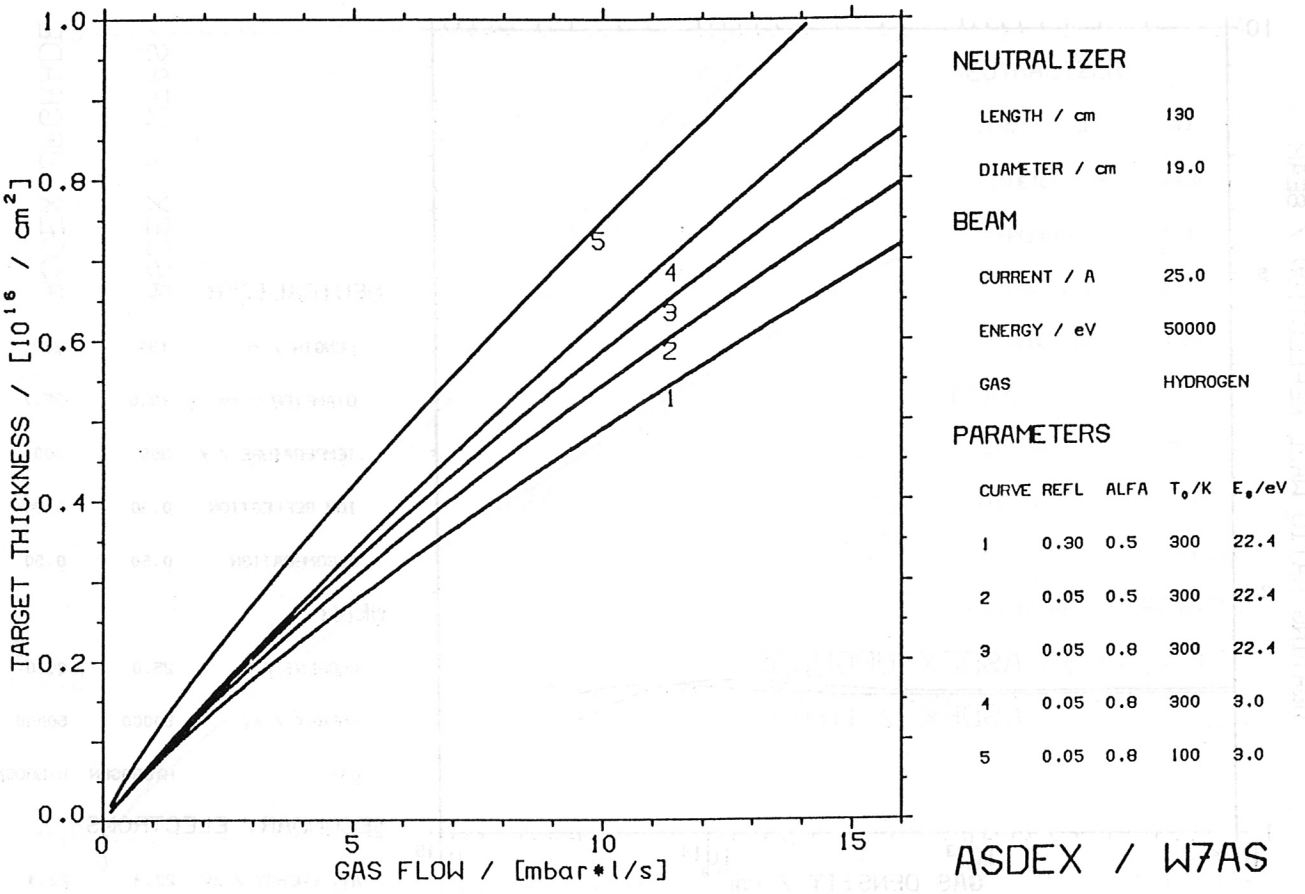
TARGET THICKNESS / [10^16 / cm^2]
GAS FLOW / [mbar*l/s]
1.0
0.8
0.6
0.4
0.2
0.0
0
5
10
15
1
2
3
4
5
NEUTRALIZER
LENGTH / cm 130
DIAMETER / cm 19.0
BEAM
CURRENT / A 25.0
ENERGY / eV 50000
GAS HYDROGEN
PARAMETERS
CURVE REFL ALFA T0/K E0/eV
1 0.30 0.5 300 22.4
2 0.05 0.5 300 22.4
3 0.05 0.8 300 22.4
4 0.05 0.8 300 3.0
5 0.05 0.8 100 3.0
ASDEX / W7AS

Fig. 11

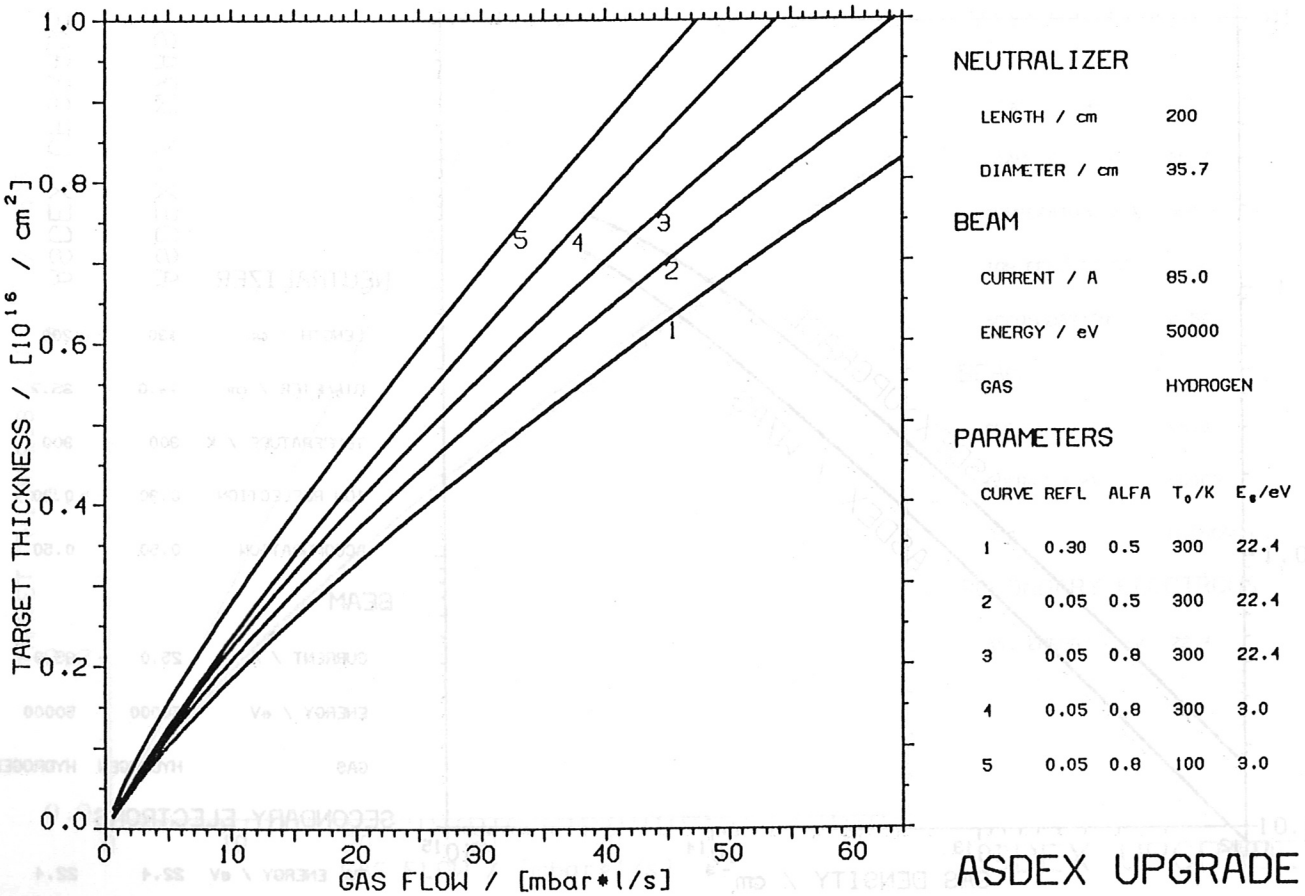
TARGET THICKNESS / [10^16 / cm^2]
GAS FLOW / [mbar*l/s]
1.0
0.8
0.6
0.4
0.2
0.0
0
10
20
30
40
50
60
1
2
3
4
5
NEUTRALIZER
LENGTH / cm 200
DIAMETER / cm 35.7
BEAM
CURRENT / A 85.0
ENERGY / eV 50000
GAS HYDROGEN
PARAMETERS
CURVE REFL ALFA T0/K E0/eV
1 0.30 0.5 300 22.4
2 0.05 0.5 300 22.4
3 0.05 0.8 300 22.4
4 0.05 0.8 300 3.0
5 0.05 0.8 100 3.0
ASDEX UPGRADE

Fig. 12

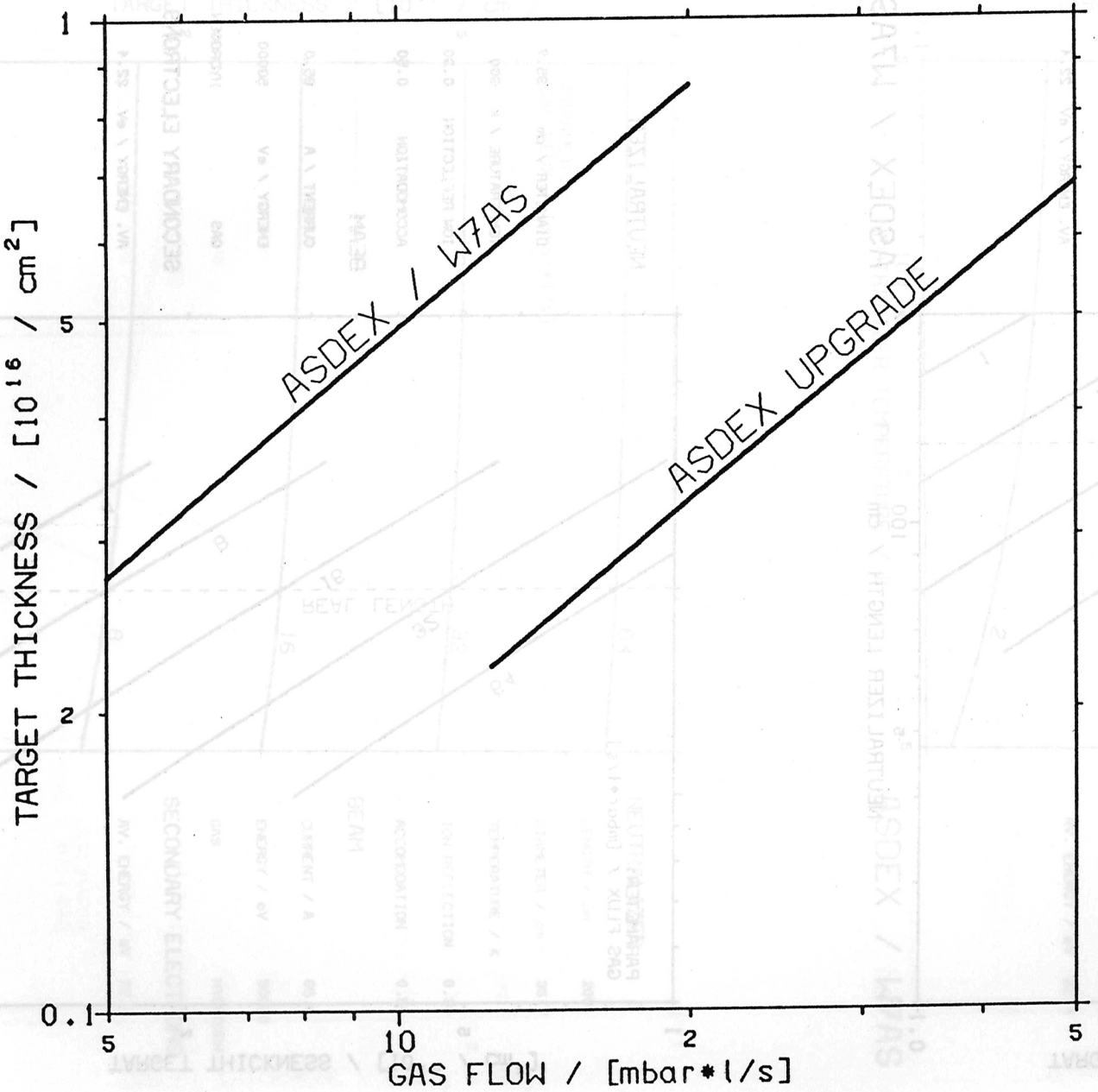

NEUTRALIZER	ASDEX / W7AS	ASDEX UPGRADE
LENGTH / cm	130	200
DIAMETER / cm	19.0	35.7
TEMPERATURE / K	300	300
ION REFLECTION	0.30	0.30
ACCOMODATION	0.50	0.50
BEAM		
CURRENT / A	25.0	85.0
ENERGY / eV	50000	50000
GAS	HYDROGEN	HYDROGEN
SECONDARY ELECTRONS		
AV. ENERGY / eV	22.4	22.4

Fig. 13

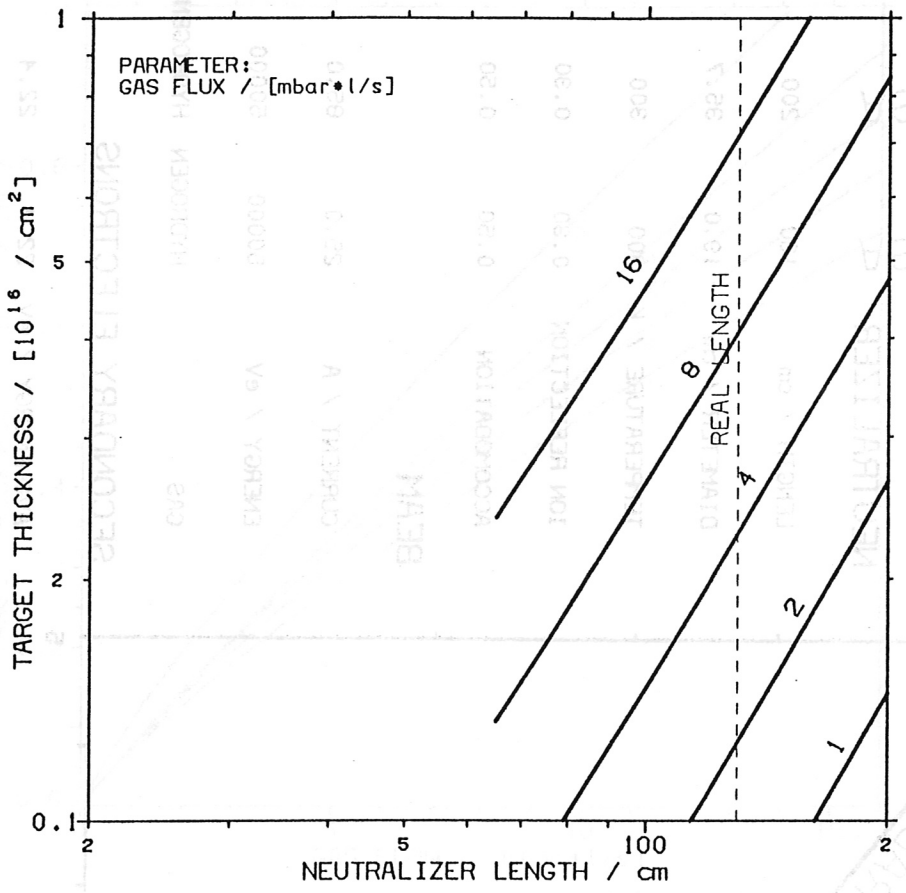

NEUTRALIZER

DIAMETER / cm	19.0
TEMPERATURE / K	300
ION REFLECTION	0.30
ACCOMODATION	0.50

BEAM

CURRENT / A	25.0
ENERGY / eV	50000
GAS	HYDROGEN

SECONDARY ELECTRONS

AV. ENERGY / eV	22.4

ASDEX / W7AS

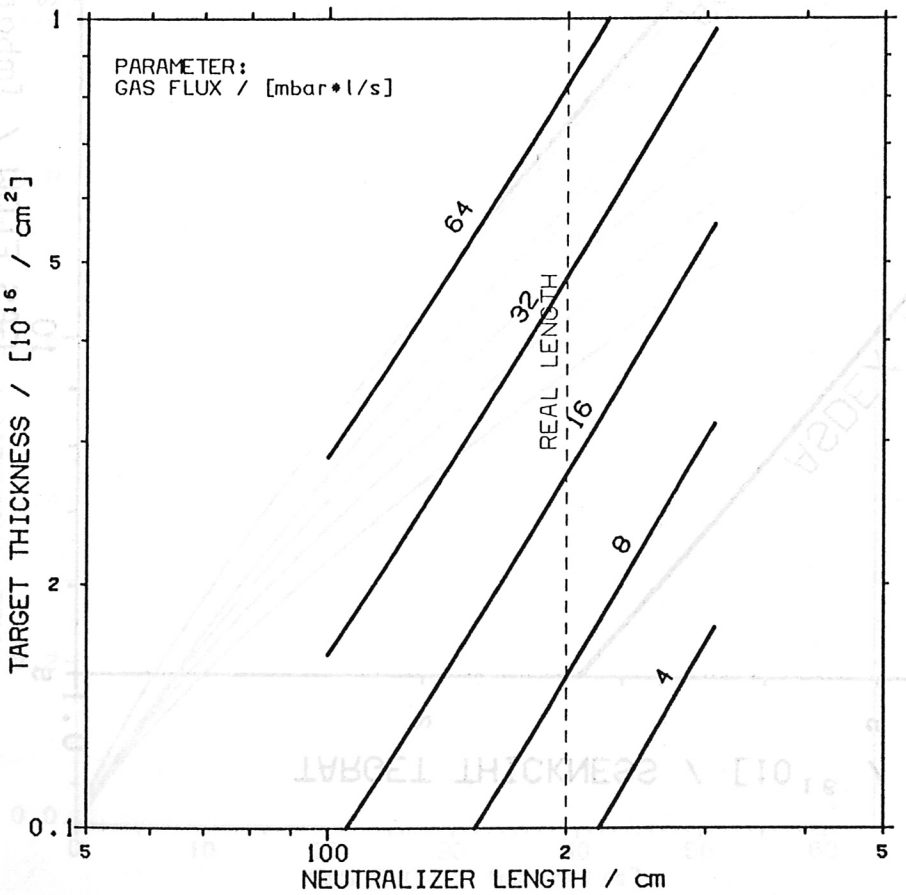

NEUTRALIZER

DIAMETER / cm	35.7
TEMPERATURE / K	300
ION REFLECTION	0.30
ACCOMODATION	0.50

BEAM

CURRENT / A	85.0
ENERGY / eV	50000
GAS	HYDROGEN

SECONDARY ELECTRONS

AV. ENERGY / eV	22.4

ASDEX UPGRADE

Fig. 14

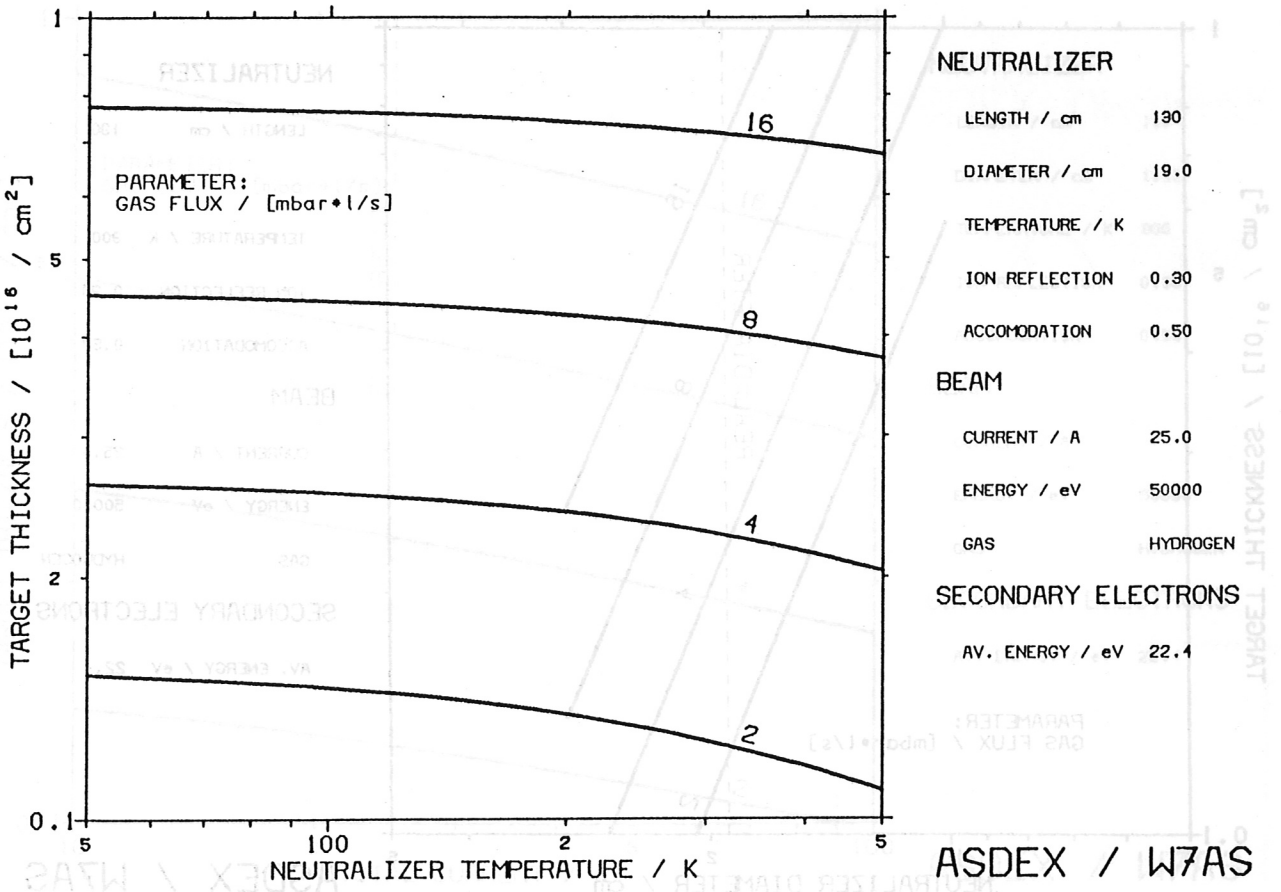
TARGET THICKNESS / [10^16 / cm^2]
1
5
2
0.1
PARAMETER:
GAS FLUX / [mbar*l/s]
16
8
4
2
5
100
2
5
NEUTRALIZER TEMPERATURE / K
NEUTRALIZER
LENGTH / cm 130
DIAMETER / cm 19.0
TEMPERATURE / K
ION REFLECTION 0.30
ACCOMODATION 0.50
BEAM
CURRENT / A 25.0
ENERGY / eV 50000
GAS HYDROGEN
SECONDARY ELECTRONS
AV. ENERGY / eV 22.4
ASDEX / W7AS

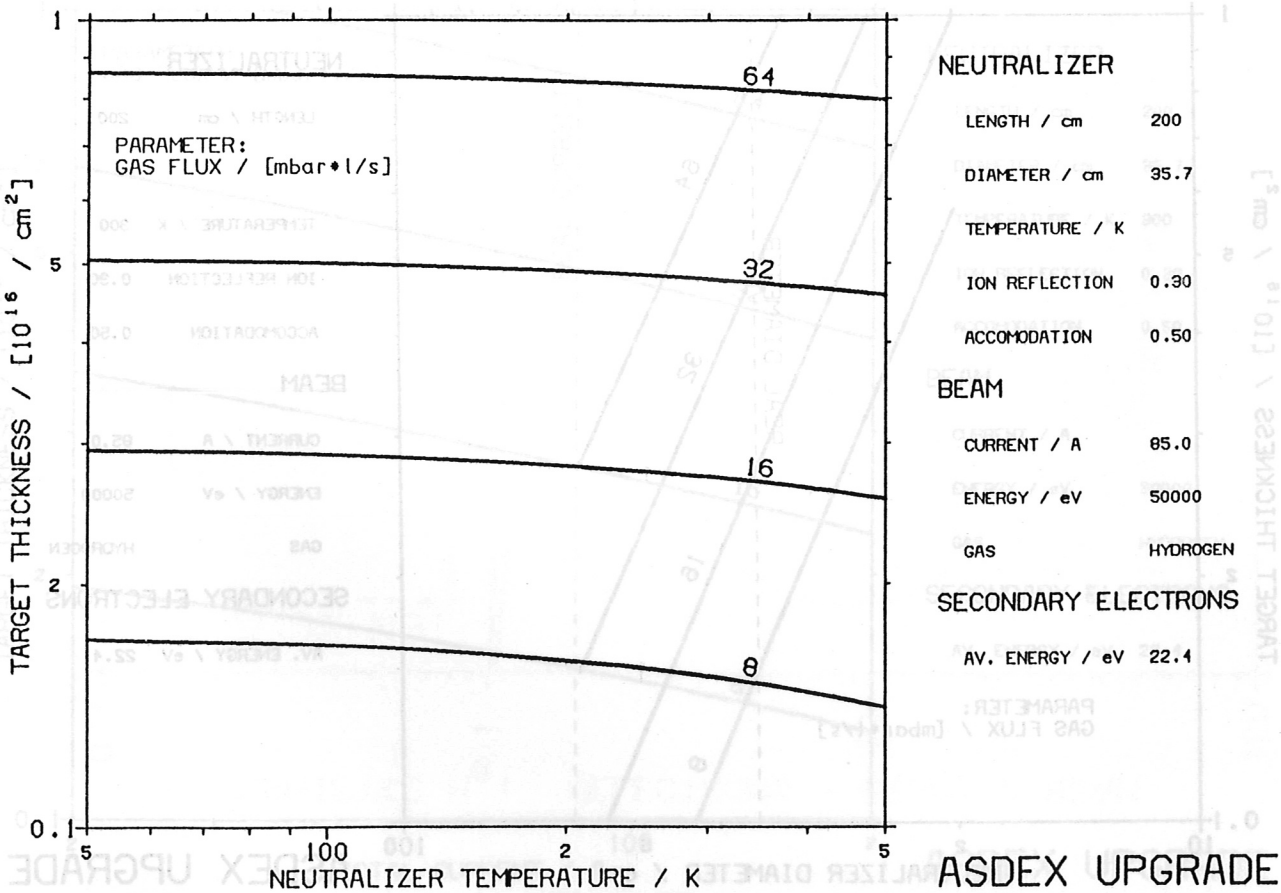
TARGET THICKNESS / [10^16 / cm^2]
1
5
2
0.1
PARAMETER:
GAS FLUX / [mbar*l/s]
64
32
16
8
5
100
2
5
NEUTRALIZER TEMPERATURE / K
NEUTRALIZER
LENGTH / cm 200
DIAMETER / cm 35.7
TEMPERATURE / K
ION REFLECTION 0.30
ACCOMODATION 0.50
BEAM
CURRENT / A 65.0
ENERGY / eV 50000
GAS HYDROGEN
SECONDARY ELECTRONS
AV. ENERGY / eV 22.4
ASDEX UPGRADE

Fig. 15

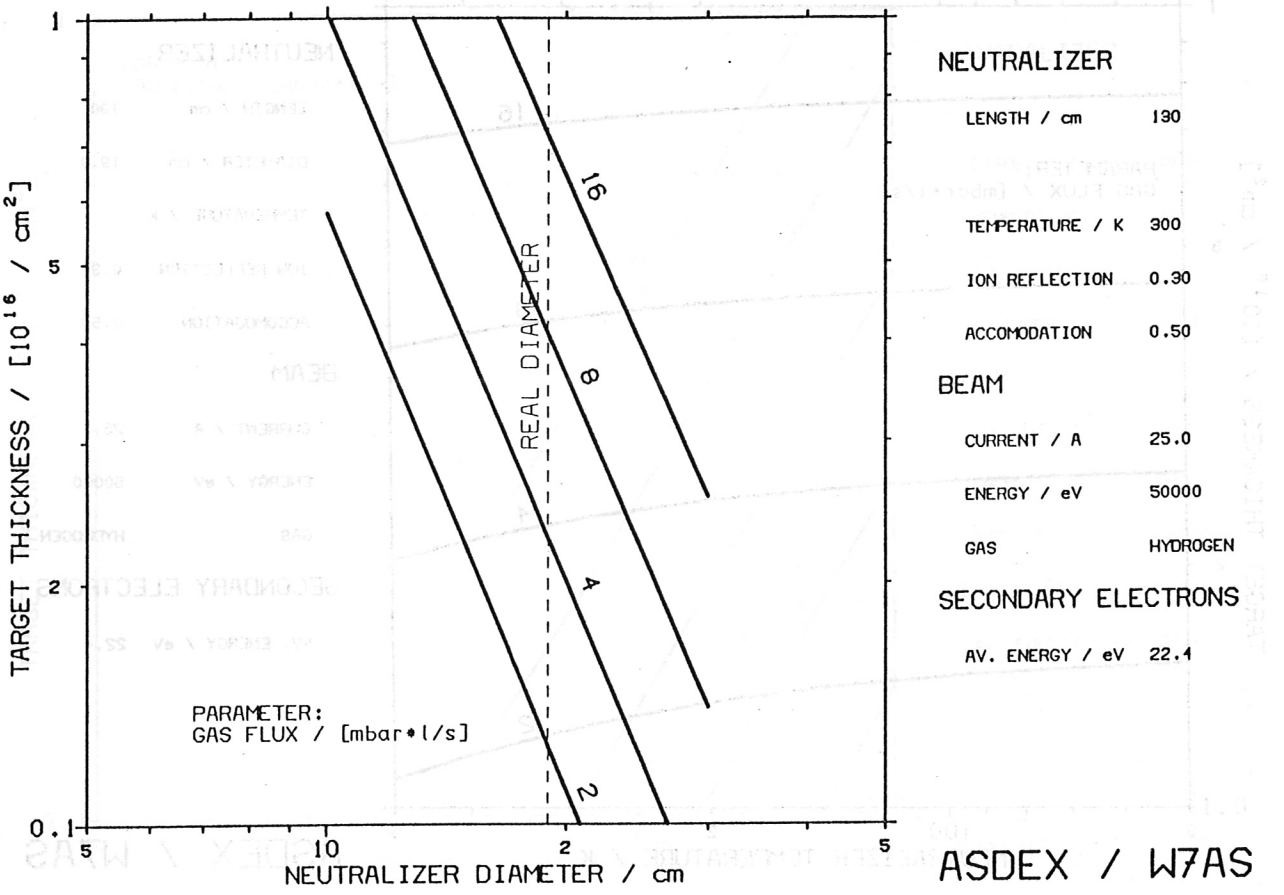
TARGET THICKNESS / [10¹⁶ / cm²]
1
5
2
0.1
16
8
4
2
REAL DIAMETER
PARAMETER:
GAS FLUX / [mbar•l/s]
5
10
2
5
NEUTRALIZER DIAMETER / cm
NEUTRALIZER
LENGTH / cm 130
TEMPERATURE / K 300
ION REFLECTION 0.30
ACCOMODATION 0.50
BEAM
CURRENT / A 25.0
ENERGY / eV 50000
GAS HYDROGEN
SECONDARY ELECTRONS
AV. ENERGY / eV 22.4
ASDEX / W7AS

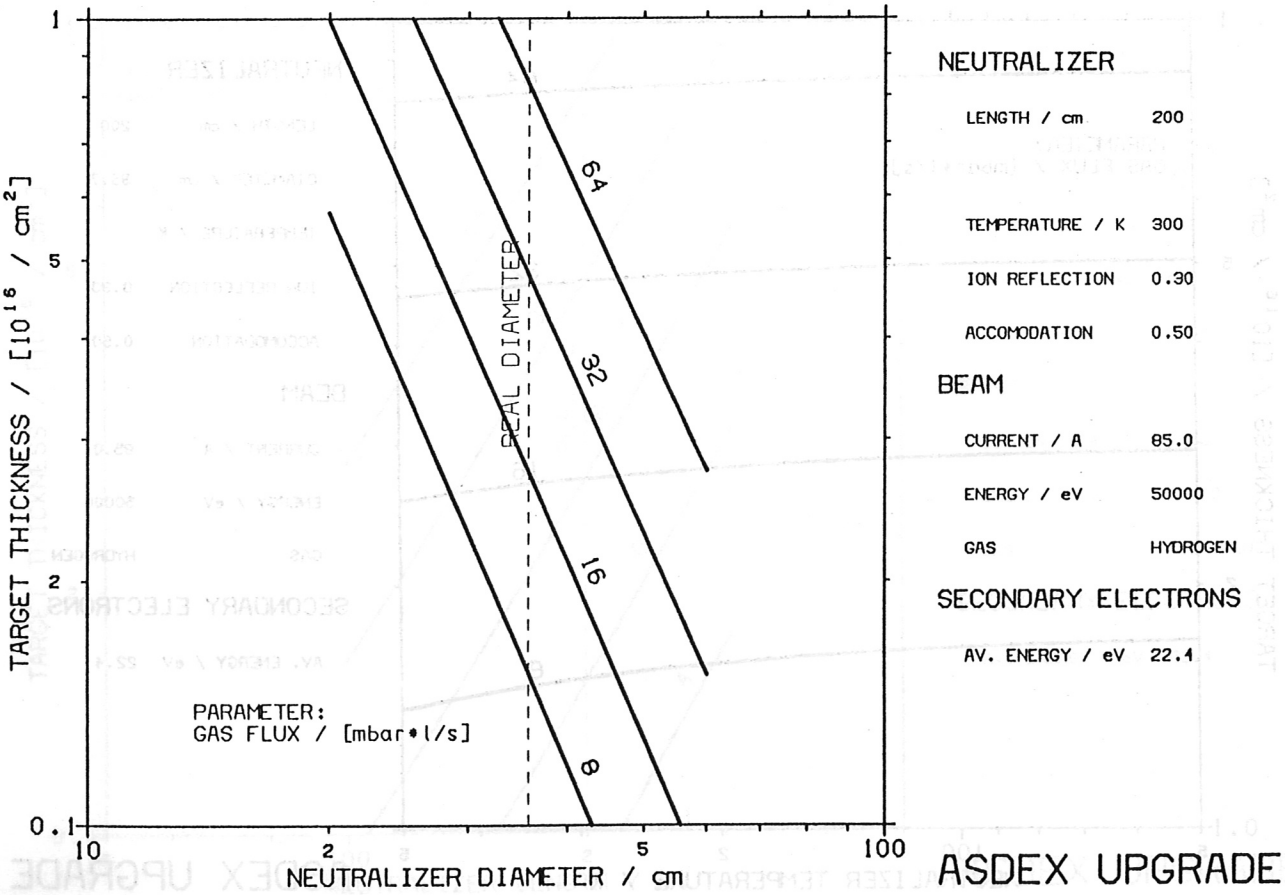
TARGET THICKNESS / [10¹⁶ / cm²]
1
5
2
0.1
64
32
16
8
REAL DIAMETER
PARAMETER:
GAS FLUX / [mbar•l/s]
10
2
5
100
NEUTRALIZER DIAMETER / cm
NEUTRALIZER
LENGTH / cm 200
TEMPERATURE / K 300
ION REFLECTION 0.30
ACCOMODATION 0.50
BEAM
CURRENT / A 65.0
ENERGY / eV 50000
GAS HYDROGEN
SECONDARY ELECTRONS
AV. ENERGY / eV 22.4
ASDEX UPGRADE

Fig. 16

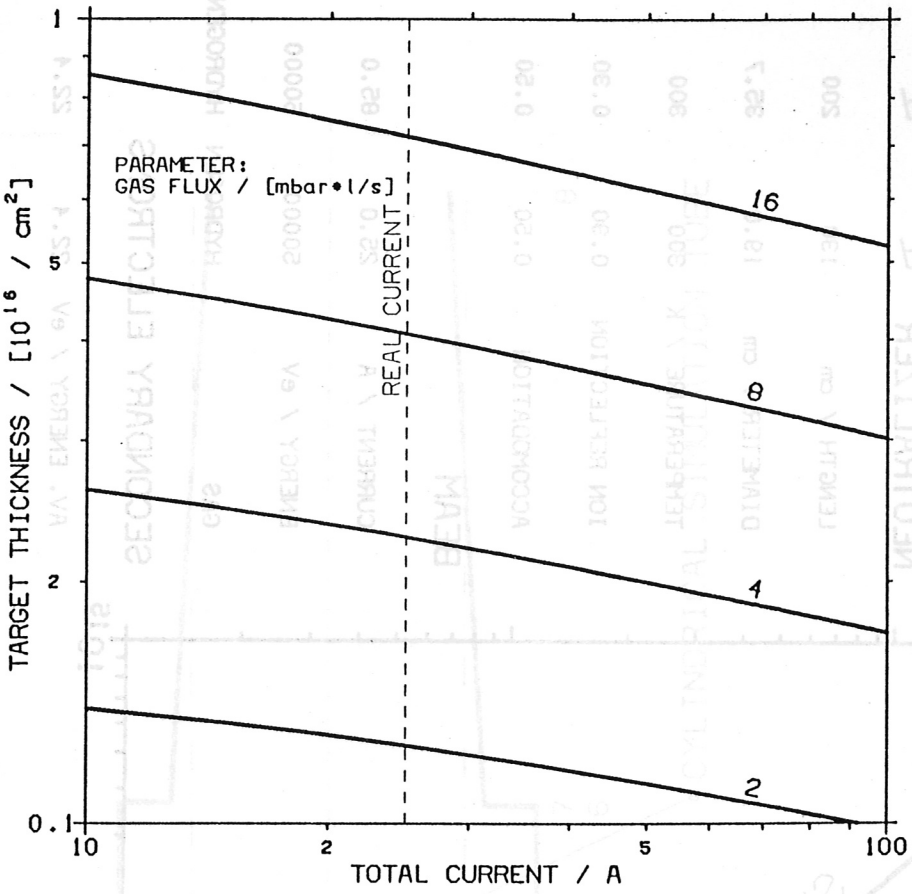

NEUTRALIZER

LENGTH / cm	130
DIAMETER / cm	19.0
TEMPERATURE / K	300
ION REFLECTION	0.30
ACCOMODATION	0.50

BEAM

CURRENT / A	
ENERGY / eV	50000
GAS	HYDROGEN

SECONDARY ELECTRONS

AV. ENERGY / eV	22.4

ASDEX / W7AS

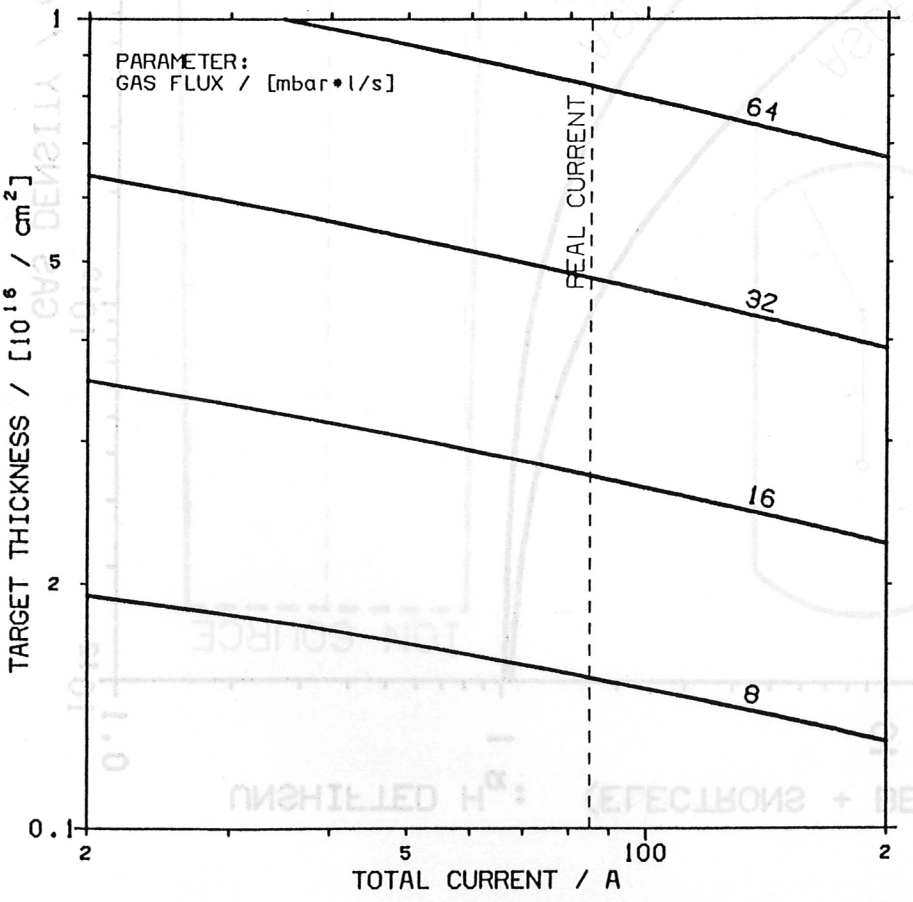

NEUTRALIZER

LENGTH / cm	200
DIAMETER / cm	35.7
TEMPERATURE / K	300
ION REFLECTION	0.30
ACCOMODATION	0.50

BEAM

CURRENT / A	
ENERGY / eV	50000
GAS	HYDROGEN

SECONDARY ELECTRONS

AV. ENERGY / eV	22.4

ASDEX UPGRADE

Fig. 17

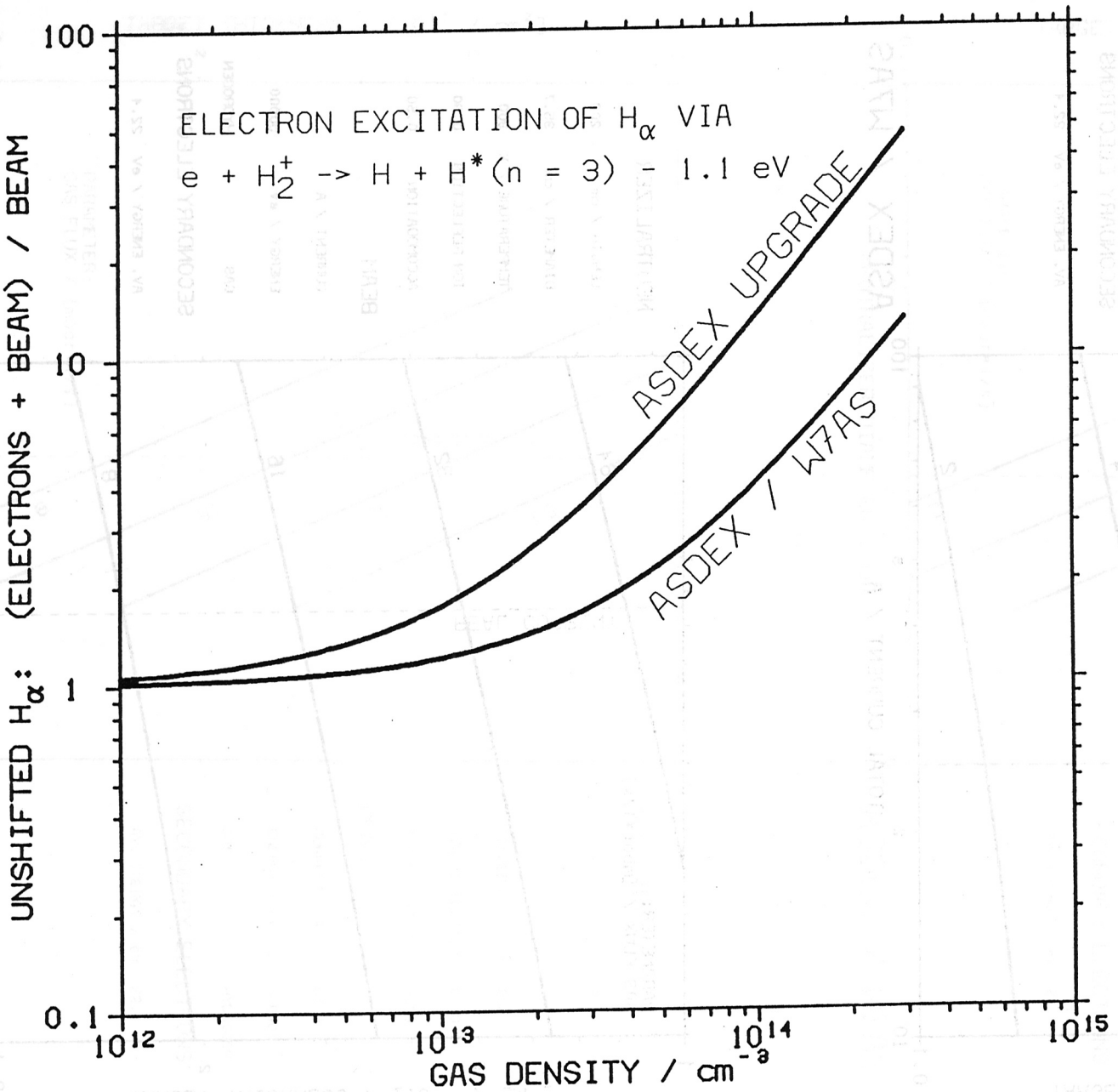

NEUTRALIZER	ASDEX / W7AS	ASDEX UPGRADE
LENGTH / cm	130	200
DIAMETER / cm	19.0	35.7
TEMPERATURE / K	300	300
ION REFLECTION	0.30	0.30
ACCOMODATION	0.50	0.50
BEAM		
CURRENT / A	25.0	85.0
ENERGY / eV	50000	50000
GAS	HYDROGEN	HYDROGEN
SECONDARY ELECTRONS		
AV. ENERGY / eV	22.4	22.4

Fig. 18

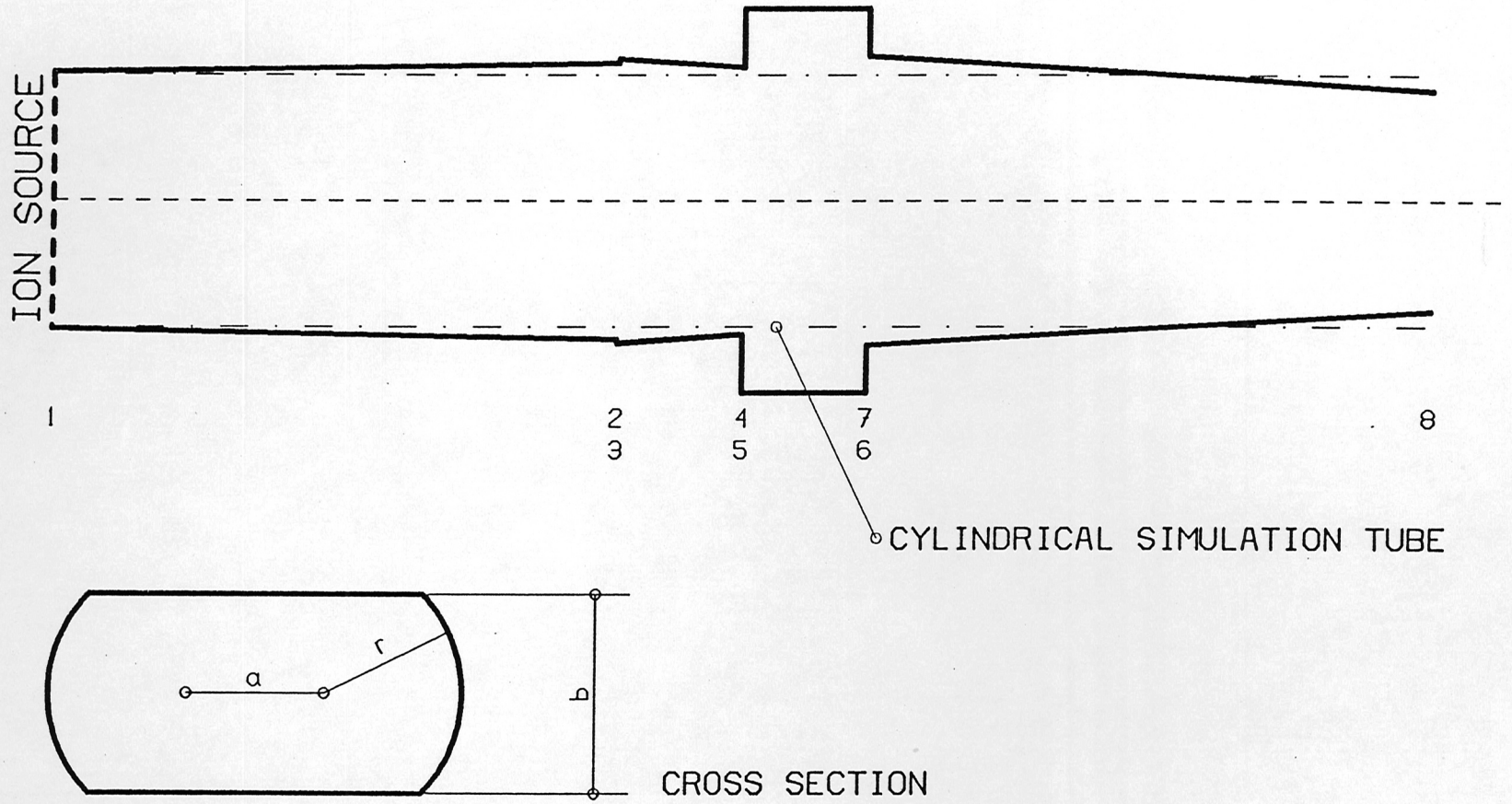

ASDEX UPGRADE NEUTRALIZER

Fig. 19